The dynamic stiffness matrix based on the extended separation-of-variables type solution for the free vibration of orthotropic rectangular thin plates

Shiyi Mei[a], Colin Caprani[a,*], Daniel Cantero[b]

[a] *Department of Civil Engineering, Monash University, Melbourne, Victoria, Australia*
[b] *Department of Structural Engineering, Norwegian University of Science & Technology NTNU, Trondheim, Norway*

Abstract

The dynamic stiffness matrix (DSM) based on the extended separation-of-variables (SOV) type mode solution is developed for the free vibration analysis of an orthotropic rectangular thin plate with general homogeneous boundary conditions. The method combines the advantages of the DSM method and the SOV method. The SOV type solution satisfies the governing differential equation derived from Rayleigh's principle and is used to formulate the dynamic stiffness matrices. Owing to the characteristics of the SOV type solution, the fully clamped boundary condition problem associated with the Wittrick–Williams algorithm is resolved. The enhanced algorithm is further proposed to solve dynamic stiffness matrices, rather than solving eigenvalue equations. A numerical technique for mode shape computation is also introduced. The accuracy of the proposed method is validated through numerical experiments.

1. Introduction

Rectangular plates play an important role in various engineering fields, including civil, mechanical, and aerospace engineering [3]. The free vibration of plates has been a fundamental research problem for over two centuries.

*Corresponding author

Email addresses: `shiyi.mei1@monash.edu` (Shiyi Mei), `colin.caprani@monash.edu` (Colin Caprani), `daniel.cantero@ntnu.no` (Daniel Cantero)

The earliest exact solutions for this problem are the Navier [21] and Levy [14] solutions, which require at least one pair of opposite edges to be simply supported or guided. To solve problems with other boundary conditions, approximate solutions such as the Rayleigh–Ritz method [13] and the Galerkin method [12] have been widely applied. For these approximation methods, beam functions, polynomials, trigonometric functions, and their combinations [16] are commonly used as the assumed approximate functions. The accuracy of these solutions depends on how well the assumed approximate functions represent the displacement of the plate.

Besides the approximation methods, several analytical methods have been developed over the past decades, including the Kantorovich-Krylov method [9, 10], the symplectic eigenfunction expansion method [32, 25], the separation-of-variable (SOV) method [29], the dynamic stiffness matrix (DSM) method [2], and series expansion-based methods [24]. The series expansion-based methods include the superposition method [22, 7], Fourier series method [11, 17], the finite integral transform method [15, 33], and other series methods. These methods represent the plate displacement in terms of an infinite series and mostly are capable of handling any general boundary conditions. However, sufficient truncation of the series is required to ensure the accuracy and convergence of the results, and the eigenvalue equation is generally difficult to express explicitly. Therefore, solving the corresponding eigenvalue problem can be computationally expensive.

Despite being a powerful method for the dynamic analysis of plate assemblies, the finite element method (FEM) requires a sufficient number of elements and is computationally expensive to accurately capture higher-order modes. Thus, the DSM method was developed as an accurate and efficient analytical approach to alternatively solve complex plate structures [4, 5]. The DSM can be considered as an analytical FEM since the mode functions of the plate are expressed by analytical solutions, where Levy-type solution [6] or components of infinite Fourier series [1, 19] are applied. To avoid solving the cumbersome transcendental frequency equation directly, the Wittrick-Williams (W-W) algorithm [23] is applied to the eigenvalue problem. The W-W algorithm determines the lower and upper bounds of natural frequencies rather than solving the frequency equation directly. Thus, the DSM has the potential to be effectively and systematically solved using the W-W algorithm. However, a critical part in applying the W-W algorithm is to priorly determine all natural frequencies of the fully clamped structure within the interested frequency range. Strategies such as using a sufficiently fine mesh or including a sufficient number of terms in series expansions [1] can ensure that all fully clamped frequencies are accounted for, thereby maintaining the accuracy of the algorithm. However, these approaches are computationally expensive and complex, posing a significant obstacle to the wider adoption and application of the DSM method based on the W-W algorithm [8]. To resolve the fully clamped plate problem, Liu and Banerjee [18] suggested that the frequencies can be indirectly obtained from the simply supported plate problem, where the Navier solution serves as the analytical solution. This provides a significant enhancement to the W-W algorithm, increasing the efficiency of applying DSM methods. However, the solutions are not explicit and closed-form, but are expressed in an infinite series form, where a sufficient number of truncation terms is required to ensure accuracy.

Inspired by the Navier and Levy solutions, Xing and Liu [29] proposed the separation-of-variables (SOV) method, which provides concise and explicit eigensolutions. The mode shape function has a separable form, $\phi(x)\psi(y)$, requiring only one $\phi(x)$ and one $\psi(y)$ for each mode order, allowing each eigenvalue equation to be explicitly expressed. However, this SOV method is not suitable to deal with plates with free boundary conditions. Therefore, an extended SOV method [26, 27] based on the Rayleigh quotient was proposed to accommodate plates with all four classical boundary conditions, i.e., simply supported, clamped, guided, and free. Based on the Rayleigh quotient model, alternative iterative and improved SOV methods have been subsequently proposed [28]. Although SOV methods provide concise closed-form analytical solutions, they require solving a specific set of highly nonlinear eigenvalue equations for each type of boundary condition. However, even when considering only the four classic homogeneous cases, it becomes evident that 55 different boundary condition combinations exist for a rectangular plate, making the process tedious.

In this study, the SOV method is extended to analyze the vibrations of plates with elastically restrained edges. The extended SOV type solution is then employed to construct the dynamic stiffness matrices, which accommodate all general homogeneous boundary conditions. By taking advantage of both the SOV and DSM methods, an enhanced W-W algorithm is developed to solve the eigenvalue problem without directly solving the eigenvalue equations. This enhanced approach resolves the challenge of determining fully clamped frequencies, a well-known limitation in the application of the W-W algorithm. In addition, a novel numerical technique has been proposed to compute the mode shape coefficients.

2. Mathematical model

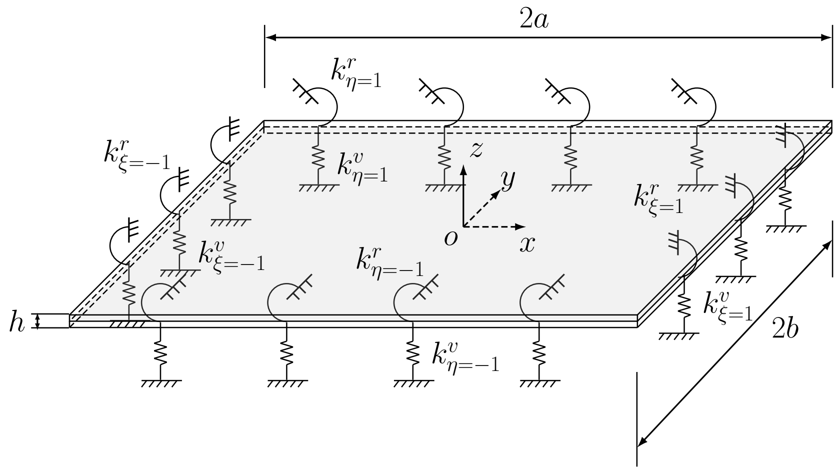

Figure 1: The orthotropic rectangular plate with all edges elastically restrained.

Consider a thin orthotropic rectangular plate of length $2a$ and width $2b$, with all four edges restrained by vertical translational springs k^v and rotational springs k^r, as shown in Figure 1. The coordinate origin is located at the center of the plate.

The governing differential equation for the free vibration of a thin orthotropic plate is given by [28]:

$$D_{11}\frac{\partial^4 w}{\partial \xi^4} + 2D_3\alpha^2\frac{\partial^4 w}{\partial \xi^2 \partial \eta^2} + D_{22}\alpha^4\frac{\partial^4 w}{\partial \eta^4} = \rho h \alpha^4 \omega^2 w, \tag{1}$$

where $\alpha = a/b$ is the aspect ratio; $\xi = x/a$ and $\eta = y/b$ are the normalized coordinates, and the bending stiffness parameters are defined as:

$$\begin{aligned} D_{11} &= \frac{E_1 h^3}{12(1-v_{12}v_{21})}, \quad D_{22} = \frac{E_2 h^3}{12(1-v_{12}v_{21})}, \\ D_{66} &= \frac{G_{12}h^3}{12}, \quad D_{12} = v_{12}D_{22} = v_{21}D_{11}, \quad D_3 = D_{12} + 2D_{66}, \end{aligned} \tag{2}$$

where ρ and h denote the mass density and thickness of the plate, respectively; E_1 and E_2 are the Young's moduli in the x- and y-directions, respectively; G_{12} is the shear modulus, and v_{12} and v_{21} are the Poisson's ratios.

Instead of solving the free vibration of the thin orthotropic plate using Equation (1), it is suggested that the vibration of the thin plate can also be solved using the Rayleigh quotient variational principle [26]:

$$\delta U_{mag} = \omega^2 \, \delta T_0, \tag{3}$$

where δ denotes variation, U_{mag} is the magnitude of the potential energy of the plate, and $\omega^2 T_0$ represents the magnitude of the kinetic energy of the plate. The potential energy of the plate can be expressed as [27]:

$$\begin{aligned} U^I = \frac{1}{2} \iint \Bigg[& D_{11} \left(\frac{\partial^2 W}{\partial x^2} \right)^2 + 2D_{12} \frac{\partial^2 W}{\partial x^2} \frac{\partial^2 W}{\partial y^2} + D_{22} \left(\frac{\partial^2 W}{\partial y^2} \right)^2 \\ & + 4D_{66} \left(\frac{\partial^2 W}{\partial x \partial y} \right)^2 \Bigg] \mathrm{d}x \, \mathrm{d}y. \end{aligned} \tag{4}$$

And the kinetic energy is:

$$T = \frac{1}{2} \iint \rho h \left(\frac{\partial W}{\partial t} \right)^2 \mathrm{d}x \, \mathrm{d}y. \tag{5}$$

Assuming the solution of the deflection $W(x, y; t) = w(x, y) e^{i\omega t}$ for harmonic plate motion, where $\mathrm{i} = \sqrt{-1}$, $w(x, y)$ is the mode shape, and ω is the radial frequency. By substituting $W(x, y; t) = w(x, y) e^{i\omega t}$ into Equations (4) and (5) and expressing the system in dimensionless coordinates, we have:

$$\begin{aligned} U^I_{\mathrm{mag}} = \frac{ab}{2} \iint \Bigg[& \frac{D_{11}}{a^4} \left(\frac{\partial^2 w}{\partial \xi^2} \right)^2 + \frac{2D_{12}}{a^2 b^2} \frac{\partial^2 w}{\partial \xi^2} \frac{\partial^2 w}{\partial \eta^2} + \frac{D_{22}}{b^4} \left(\frac{\partial^2 w}{\partial \eta^2} \right)^2 \\ & + \frac{4D_{66}}{a^2 b^2} \left(\frac{\partial^2 w}{\partial \xi \partial \eta} \right)^2 \Bigg] \mathrm{d}\xi \, \mathrm{d}\eta, \end{aligned} \tag{6}$$

and

$$T = \omega^2 \frac{ab}{2} \rho h \iint w^2 \, \mathrm{d}\xi \, \mathrm{d}\eta = \omega^2 T_0, \tag{7}$$

The separable form of the mode shape function $w(\xi, \eta)$ is given by:

$$w(\xi, \eta) = \phi(\xi) \psi(\eta), \tag{8}$$

where $\phi(\xi)$ and $\psi(\eta)$ can be expressed as:

$$\phi(\xi) = A_1 \sin(\alpha_1 \xi) + A_2 \cos(\alpha_1 \xi) + A_3 \sinh(\beta_1 \xi) + A_4 \cosh(\beta_1 \xi), \tag{9a}$$
$$\psi(\eta) = B_1 \sin(\alpha_2 \eta) + B_2 \cos(\alpha_2 \eta) + B_3 \sinh(\beta_2 \eta) + B_4 \cosh(\beta_2 \eta). \tag{9b}$$

Based on Equation (3), the frequencies ω_x and ω_y, corresponding to the mode shapes $\phi(\xi)$ and $\psi(\eta)$, respectively, are assumed to be independent of each other.

2.1. Dynamic stiffness matrix corresponding to ω_x

For given general homogeneous boundary conditions, we can first assume that the mode shape $\psi(\eta)$ corresponding to the y-direction is known. Supposing the edges of the plate in both the x- and y-directions are elastically restrained by homogeneous vertical translational and rotational springs. The vertical translational and rotational springs at the $\xi = -1$ end are defined as $k^v_{\xi=-1}$ and $k^r_{\xi=-1}$, respectively, and at the $\xi = 1$ end as $k^v_{\xi=1}$ and $k^r_{\xi=1}$, respectively. Thus, the potential energy along the supported edge in the x-direction can be expressed by:

$$\begin{aligned} U^{II} = &\int \left[k^r_{\xi=-1} \left(\frac{\partial W}{\partial x} \right)^2 + k^v_{\xi=-1} (W)^2 \right]_{x=-a} \mathrm{d}y \\ &+ \int \left[k^r_{\xi=1} \left(\frac{\partial W}{\partial x} \right)^2 + k^v_{\xi=1} (W)^2 \right]_{x=a} \mathrm{d}y. \end{aligned} \tag{10}$$

From Equation (10), the magnitude of total potential energy along the edges in the x-direction is obtained as:

$$\begin{aligned} U^{II}_{mag} = ab &\int \left[\frac{k^r_{\xi=-1}}{a^3} \left(\frac{\partial w}{\partial \xi} \right)^2 + \frac{k^v_{\xi=-1}}{a} (w)^2 \right]_{\xi=-1} \mathrm{d}\eta \\ &+ ab \int \left[\frac{k^r_{\xi=1}}{a^3} \left(\frac{\partial w}{\partial \xi} \right)^2 + \frac{k^v_{\xi=1}}{a} (w)^2 \right]_{\xi=1} \mathrm{d}\eta. \end{aligned} \tag{11}$$

The magnitude of potential energy of the plate in the x-direction can be obtained from Equations (6) and (11) as:

$$
\begin{aligned}
U_{mag} &= U_{mag}^{I} + U_{mag}^{II} \\
&= \frac{ab}{2} \iint \left[\frac{D_{11}}{a^4} \left(\frac{\partial^2 w}{\partial \xi^2} \right)^2 + \frac{2D_{12}}{a^2 b^2} \frac{\partial^2 w}{\partial \xi^2} \frac{\partial^2 w}{\partial \eta^2} + \frac{D_{22}}{b^4} \left(\frac{\partial^2 w}{\partial \eta^2} \right)^2 \right. \\
&\quad \left. + \frac{4D_{66}}{a^2 b^2} \left(\frac{\partial^2 w}{\partial \xi \partial \eta} \right)^2 \right] \mathrm{d}\xi \, \mathrm{d}\eta + ab \int \left[\frac{k^r_{\xi=1}}{a^3} \left(\frac{\partial w}{\partial \xi} \right)^2 + \frac{k^v_{\xi=1}}{a} (w)^2 \right]_{\xi=1} \mathrm{d}\eta \\
&\quad + ab \int \left[\frac{k^r_{\xi=-1}}{a^3} \left(\frac{\partial w}{\partial \xi} \right)^2 + \frac{k^v_{\xi=-1}}{a} (w)^2 \right]_{\xi=-1} \mathrm{d}\eta
\end{aligned}
\tag{12}
$$

By substituting Equation (8) into Equation (12), we have:

$$
\begin{aligned}
U_{mag} &= U_{mag}^{I} + U_{mag}^{II} \\
&= \frac{ab}{2} \int_{-1}^{1} \left[\frac{D_{11}}{a^4} I_1 \left(\frac{\mathrm{d}^2 \phi}{\mathrm{d}\xi^2} \right)^2 + \frac{2D_{12}}{a^2 b^2} I_2 \frac{\mathrm{d}^2 \phi}{\mathrm{d}\xi^2} \phi + \frac{D_{22}}{b^4} I_4 \phi^2 \right. \\
&\quad \left. + \frac{4D_{66}}{a^2 b^2} I_3 \left(\frac{\mathrm{d}\phi}{\mathrm{d}\xi} \right)^2 \right] \mathrm{d}\xi + abI_1 \left[\frac{k^r_{\xi=-1}}{a^3} \left(\frac{\mathrm{d}\phi}{\mathrm{d}\xi} \right)^2 + \frac{k^v_{\xi=-1}}{a} (\phi)^2 \right]_{\xi=-1} \\
&\quad + abI_1 \left[\frac{k^r_{\xi=1}}{a^3} \left(\frac{\mathrm{d}\phi}{\mathrm{d}\xi} \right)^2 + \frac{k^v_{\xi=1}}{a} (\phi)^2 \right]_{\xi=1},
\end{aligned}
\tag{13}
$$

where the integral parameters are defined as:

$$
\begin{aligned}
I_1 &= \int_{-1}^{1} \psi^2 \, \mathrm{d}\eta, \\
I_2 &= \int_{-1}^{1} \left(\frac{\mathrm{d}^2 \psi}{\mathrm{d}\eta^2} \psi \right) \mathrm{d}\eta, \\
I_3 &= \int_{-1}^{1} \left(\frac{\mathrm{d}\psi}{\mathrm{d}\eta} \right)^2 \mathrm{d}\eta, \\
I_4 &= \int_{-1}^{1} \left(\frac{\mathrm{d}^2 \psi}{\mathrm{d}\eta^2} \right)^2 \mathrm{d}\eta.
\end{aligned}
\tag{14}
$$

By taking Equation (8) into account, the coefficient T_0 of the kinetic energy from Equation (7) for the plate can be expressed as:

$$T_0 = \frac{ab}{2}\rho h \iint w^2 \,\mathrm{d}\xi \,\mathrm{d}\eta = \frac{ab}{2}\rho h I_1 \int_{-1}^{1} \phi^2 \,\mathrm{d}\xi. \tag{15}$$

Take the Rayleigh principle in the form:

$$\delta U_{mag} = \omega_x^2 \,\delta T_0. \tag{16}$$

By substituting Equations (13) and (15) into Equation (16), and relieving $\delta\phi$ and $\delta\frac{\mathrm{d}\phi}{\mathrm{d}\xi}$ in Equation (16) by variation calculus, yields:

$$\begin{aligned} 0 = &\int_{-1}^{1} \left[\frac{D_{11}}{a^4} I_1 \frac{\mathrm{d}^4\phi}{\mathrm{d}\xi^4} + \left(\frac{2D_{12}}{a^2b^2} I_2 - \frac{4D_{66}}{a^2b^2} I_3 \right) \frac{\mathrm{d}^2\phi}{\mathrm{d}\xi^2} \right. \\ &\left. + \left(\frac{D_{22}}{b^4} I_4 - \omega_x^2 \rho h I_1 \right) \phi \right] \delta\phi \,\mathrm{d}\xi \\ &+ \frac{2k^v_{\xi=-1}}{a} I_1 \Big(\phi\delta\phi\Big)_{\xi=-1} + \frac{2k^v_{\xi=1}}{a} I_1 \Big(\phi\delta\phi\Big)_{\xi=1} \\ &+ \left[\left(\frac{4D_{66}}{a^2b^2} I_3 - \frac{D_{12}}{a^2b^2} I_2 \right) \frac{\mathrm{d}\phi}{\mathrm{d}\xi} - \frac{D_{11}}{a^4} I_1 \frac{\mathrm{d}^3\phi}{\mathrm{d}\xi^3} \right] \delta\phi \Big|_{\xi=-1}^{\xi=1} \\ &+ \left(\frac{D_{12}}{a^2b^2} I_2 \phi + \frac{D_{11}}{a^4} I_1 \frac{\mathrm{d}^2\phi}{\mathrm{d}\xi^2} \right) \delta \frac{\mathrm{d}\phi}{\mathrm{d}\xi} \Big|_{\xi=-1}^{\xi=1} \\ &+ \frac{2k^r_{\xi=-1}}{a^3} I_1 \left(\frac{\mathrm{d}\phi}{\mathrm{d}\xi} \delta \frac{\mathrm{d}\phi}{\mathrm{d}\xi} \right)_{\xi=-1} + \frac{2k^r_{\xi=1}}{a^3} I_1 \left(\frac{\mathrm{d}\phi}{\mathrm{d}\xi} \delta \frac{\mathrm{d}\phi}{\mathrm{d}\xi} \right)_{\xi=1}. \end{aligned} \tag{17}$$

Thus, the governing differential equation in the x-direction can be obtained from the integration part in Equation (17):

$$\frac{\mathrm{d}^4\phi}{\mathrm{d}\xi^4} + 2\alpha^2 \left(\frac{D_{12}I_2}{D_{11}I_1} - 2\frac{D_{66}I_3}{D_{11}I_1} \right) \frac{\mathrm{d}^2\phi}{\mathrm{d}\xi^2} + \left(\alpha^4 \frac{D_{22}I_4}{D_{11}I_1} - a^4\Omega_x^4 \right) \phi = 0, \tag{18}$$

where $\Omega_x = \sqrt[4]{\omega_x^2 \rho h / D_{11}}$. By substituting $\phi(\xi) = Ae^{\mu\xi}$ into Equation (18), yields:

$$\mu^4 + 2\alpha^2 \left(\frac{D_{12}I_2}{D_{11}I_1} - 2\frac{D_{66}I_3}{D_{11}I_1} \right) \mu^2 + \left(\alpha^4 \frac{D_{22}I_4}{D_{11}I_1} - a^4\Omega_x^4 \right) = 0. \tag{19}$$

The solution for μ can be expressed as:

$$\mu_{1,2} = \pm i\alpha_1, \qquad \mu_{3,4} = \pm\beta_1, \tag{20}$$

where,

$$\alpha_1 = \alpha\sqrt{\sqrt{\left(\frac{D_{12}I_2}{D_{11}I_1} - 2\frac{D_{66}I_3}{D_{11}I_1}\right)^2 - \frac{D_{22}I_4}{D_{11}I_1} + b^4\Omega_x^4} + \frac{D_{12}I_2}{D_{11}I_1} - 2\frac{D_{66}I_3}{D_{11}I_1}}, \tag{21a}$$

$$\beta_1 = \alpha\sqrt{\sqrt{\left(\frac{D_{12}I_2}{D_{11}I_1} - 2\frac{D_{66}I_3}{D_{11}I_1}\right)^2 - \frac{D_{22}I_4}{D_{11}I_1} + b^4\Omega_x^4} - \frac{D_{12}I_2}{D_{11}I_1} + 2\frac{D_{66}I_3}{D_{11}I_1}}. \tag{21b}$$

The boundary conditions along the edges in the x-direction can be obtained from the remaining $\delta\phi$ and $\delta\frac{\mathrm{d}\phi}{\mathrm{d}\xi}$ parts in Equation (17). The shear force equilibrium can be obtained from the $\delta\phi$ part:

$$\begin{aligned}\left[\left(\frac{4D_{66}}{a^2b^2}I_3 - \frac{D_{12}}{a^2b^2}I_2\right)\frac{\mathrm{d}\phi}{\mathrm{d}\xi} - \frac{D_{11}}{a^4}I_1\frac{\mathrm{d}^3\phi}{\mathrm{d}\xi^3}\right]\Bigg|_{\xi=-1}^{\xi=1}\\ + \frac{2k^v_{\xi=-1}}{a}I_1\left(\phi\right)_{\xi=-1} + \frac{2k^v_{\xi=1}}{a}I_1\left(\phi\right)_{\xi=1} = 0,\end{aligned} \tag{22}$$

and from the $\delta\frac{\mathrm{d}\phi}{\mathrm{d}\xi}$ part, the bending moment equilibrium:

$$\begin{aligned}\left(\frac{D_{12}}{a^2b^2}I_2\phi + \frac{D_{11}}{a^4}I_1\frac{\partial^2\phi}{\partial\xi^2}\right)\Bigg|_{\xi=-1}^{\xi=1} + \frac{2k^r_{\xi=-1}}{a^3}I_1\left(\frac{\partial\phi}{\partial\xi}\right)_{\xi=-1}\\ + \frac{2k^r_{\xi=1}}{a^3}I_1\left(\frac{\partial\phi}{\partial\xi}\right)_{\xi=1} = 0.\end{aligned} \tag{23}$$

Thus, we can obtain the shear force and bending moment equilibrium along the edges $\xi = -1$ and $\xi = 1$ from Equations (22) and (23), respectively, as:

$$\frac{\mathrm{d}^3\phi}{\mathrm{d}\xi^3} - \alpha^2\left(\frac{4D_{66}I_3}{D_{11}I_1} - \frac{D_{12}I_2}{D_{11}I_1}\right)\frac{\mathrm{d}\phi}{\mathrm{d}\xi} + \frac{2a^3k^v_{\xi=-1}}{D_{11}}\phi = 0, \qquad \xi = -1, \tag{24a}$$

$$\frac{\mathrm{d}^2\phi}{\mathrm{d}\xi^2} + \frac{\alpha^2 D_{12}I_2}{D_{11}I_1}\phi - \frac{2ak^r_{\xi=-1}}{D_{11}}\frac{\mathrm{d}\phi}{\mathrm{d}\xi} = 0, \qquad \xi = -1, \tag{24b}$$

$$\frac{\mathrm{d}^3\phi}{\mathrm{d}\xi^3} - \alpha^2\left(\frac{4D_{66}I_3}{D_{11}I_1} - \frac{D_{12}I_2}{D_{11}I_1}\right)\frac{\mathrm{d}\phi}{\mathrm{d}\xi} - \frac{2a^3k^v_{\xi=1}}{D_{11}}\phi = 0, \qquad \xi = 1, \tag{24c}$$

$$\frac{\mathrm{d}^2\phi}{\mathrm{d}\xi^2} + \frac{\alpha^2 D_{12}I_2}{D_{11}I_1}\phi + \frac{2ak^r_{\xi=1}}{D_{11}}\frac{\mathrm{d}\phi}{\mathrm{d}\xi} = 0, \qquad \xi = 1. \tag{24d}$$

Substituting Equation (9a) into Equation (24), and denoting $k^{v*}_\xi = \frac{2a^3k^v_\xi}{D_{11}}$, $k^{r*}_\xi = \frac{2ak^r_\xi}{D_{11}}$, $S_{\alpha_1} = \sin\alpha_1$, $C_{\alpha_1} = \cos\alpha_1$, $Sh_{\alpha_1} = \sinh\alpha_1$, $Ch_{\alpha_1} = \cosh\alpha_1$,

$S_{\beta_1} = \sin\beta_1$, $C_{\beta_1} = \cos\beta_1$, $Sh_{\beta_1} = \sinh\beta_1$, and $Ch_{\beta_1} = \cosh\beta_1$, we have:

$$\begin{bmatrix} \gamma_1 C_{\alpha_1} - k^{v*}_{\xi=-1} S_{\alpha_1} & \gamma_1 S_{\alpha_1} + k^{v*}_{\xi=-1} C_{\alpha_1} & \gamma_2 Ch_{\beta_1} - k^{v*}_{\xi=-1} Sh_{\beta_1} & -\gamma_2 Sh_{\beta_1} + k^{v*}_{\xi=-1} Ch_{\beta_1} \\ \gamma_3 S_{\alpha_1} + k^{r*}_{\xi=-1}\alpha_1 C_{\alpha_1} & -\gamma_3 C_{\alpha_1} + k^{r*}_{\xi=-1}\alpha_1 S_{\alpha_1} & \gamma_4 Sh_{\beta_1} + k^{r*}_{\xi=-1}\beta_1 Ch_{\beta_1} & -\gamma_4 Ch_{\beta_1} - k^{r*}_{\xi=-1}\beta_1 Sh_{\beta_1} \\ -\gamma_1 C_{\alpha_1} + k^{v*}_{\xi=1} S_{\alpha_1} & \gamma_1 S_{\alpha_1} + k^{v*}_{\xi=1} C_{\alpha_1} & -\gamma_2 Ch_{\beta_1} + k^{v*}_{\xi=1} Sh_{\beta_1} & -\gamma_2 Sh_{\beta_1} + k^{v*}_{\xi=1} Ch_{\beta_1} \\ \gamma_3 S_{\alpha_1} + k^{r*}_{\xi=1}\alpha_1 C_{\alpha_1} & \gamma_3 C_{\alpha_1} - k^{r*}_{\xi=1}\alpha_1 S_{\alpha_1} & \gamma_4 Sh_{\beta_1} + k^{r*}_{\xi=1}\beta_1 Ch_{\beta_1} & \gamma_4 Ch_{\beta_1} + k^{r*}_{\xi=1}\beta_1 Sh_{\beta_1} \end{bmatrix} \begin{Bmatrix} A_1 \\ A_2 \\ A_3 \\ A_4 \end{Bmatrix} = \begin{Bmatrix} 0 \\ 0 \\ 0 \\ 0 \end{Bmatrix}, \tag{25}$$

or,

$$\mathbf{R}_x \mathbf{A} = \mathbf{0}, \tag{26}$$

where,

$$\begin{aligned} \gamma_1 &= -\alpha_1^3 - \alpha^2 \left(\frac{4D_{66}S_3}{D_{11}I_1} - \frac{D_{12}I_2}{D_{11}I_1} \right) \alpha_1, \\ \gamma_2 &= \beta_1^3 - \alpha^2 \left(\frac{4D_{66}S_3}{D_{11}I_1} - \frac{D_{12}I_2}{D_{11}I_1} \right) \beta_1, \\ \gamma_3 &= -\alpha_1^2 + \frac{\alpha^2 D_{12}I_2}{D_{11}I_1}, \\ \gamma_4 &= \beta_1^2 + \frac{\alpha^2 D_{12}I_2}{D_{11}I_1}. \end{aligned} \tag{27}$$

Note that the classic boundary conditions can be obtained by selecting extremely large or small spring stiffness constants. For non-trivial solutions, the characteristic equation or eigenvalue equation is obtained from the determinant of the matrix $\mathbf{R}_x$ in Equation (26), which must be zero. However, solving these transcendental equations are cunmbersome and tedious, thus the DSM is introducted to avoid the ineffective computation.

To develop its dynamic stiffness matrix, with the help of Equation (9a), the vertical displacement and rotation corresponding to the mode shape $\phi(\xi)$ along the x-direction at edges $\xi = -1$ and $\xi = 1$ can be expressed as:

$$\begin{Bmatrix} \phi_{\xi=-1} \\ \frac{\mathrm{d}\phi}{\mathrm{d}\xi}_{\xi=-1} \\ \phi_{\xi=1} \\ \frac{\mathrm{d}\phi}{\mathrm{d}\xi}_{\xi=1} \end{Bmatrix} = \begin{bmatrix} -S_{\alpha_1} & C_{\alpha_1} & -Sh_{\beta_1} & Ch_{\beta_1} \\ \alpha_1 C_{\alpha_1}/a & \alpha_1 S_{\alpha_1}/a & \beta_1 Ch_{\beta_1}/a & -\beta_1 Sh_{\beta_1}/a \\ S_{\alpha_1} & C_{\alpha_1} & Sh_{\beta_1} & Ch_{\beta_1} \\ \alpha_1 C_{\alpha_1}/a & -\alpha_1 S_{\alpha_1}/a & \beta_1 Ch_{\beta_1}/a & \beta_1 Sh_{\beta_1}/a \end{bmatrix} \begin{Bmatrix} A_1 \\ A_2 \\ A_3 \\ A_4 \end{Bmatrix}, \tag{28}$$

or,

$$\delta_x = \mathbf{Q}_x \mathbf{A}. \tag{29}$$

Note that the eigenvector $\mathbf{A}$ can be expressed by multiplying the inverse matrix $\mathbf{Q}_x^{-1}$ on the left side of Equation (29), and then substituting $\mathbf{A}$ into Equation (26), we obtain:

$$\mathbf{R}_x \mathbf{A} = \mathbf{R}_x \mathbf{Q}_x^{-1} \delta_x = \mathbf{0}. \tag{30}$$

where the dynamic stiffness matrix, denoted as $\mathbf{K}_x = \mathbf{R}_x \mathbf{Q}_x^{-1}$, can be obtained from Equation (30). This matrix can be used to compute the natural frequencies of the system instead of solving the eigenvalue equation, and the method for the computation will be given in Section 3.

2.2. Dynamic stiffness matrix corresponding to ω_y

In this section, the mode shape $\phi(\xi)$ derived in *Section* 2.1 is utilized to obtain the dynamic stiffness matrix in the y-direction. The vertical translational and rotational springs at $\eta = -1$ are denoted as $k^v_{\eta=-1}$ and $k^r_{\eta=-1}$, respectively, while those at $\eta = 1$ are represented by $k^v_{\eta=1}$ and $k^r_{\eta=1}$.

The magnitude of total potential energy along the edges in the y-direction is given by:

$$\begin{aligned} U^{III}_{mag} = ab \int \left[\frac{k^r_{\eta=-1}}{a^3} \left(\frac{\partial w}{\partial \eta} \right)^2 + \frac{k^v_{\eta=-1}}{a} w^2 \right]_{\eta=-1} \mathrm{d}\xi \\ + ab \int \left[\frac{k^r_{\eta=1}}{a^3} \left(\frac{\partial w}{\partial \eta} \right)^2 + \frac{k^v_{\eta=1}}{a} w^2 \right]_{\eta=1} \mathrm{d}\xi. \end{aligned} \tag{31}$$

The magnitude of potential energy of the plate in the y-direction can be obtained from Equations (6) and (31) as:

$$\begin{aligned} U_{mag} &= U^I_{mag} + U^{III}_{mag} \\ &= \frac{ab}{2} \iint \left[\frac{D_{11}}{a^4} \left(\frac{\partial^2 w}{\partial \xi^2} \right)^2 + \frac{2D_{12}}{a^2 b^2} \frac{\partial^2 w}{\partial \xi^2} \frac{\partial^2 w}{\partial \eta^2} + \frac{D_{22}}{b^4} \left(\frac{\partial^2 w}{\partial \eta^2} \right)^2 \right. \\ &\quad \left. + \frac{4D_{66}}{a^2 b^2} \left(\frac{\partial^2 w}{\partial \xi \partial \eta} \right)^2 \right] \mathrm{d}\xi \, \mathrm{d}\eta + ab \int \left[\frac{k^r_{\eta=1}}{b^3} \left(\frac{\partial w}{\partial \eta} \right)^2 + \frac{k^v_{\eta=1}}{b} (w)^2 \right]_{\eta=1} \mathrm{d}\xi \\ &\quad + ab \int \left[\frac{k^r_{\eta=-1}}{b^3} \left(\frac{\partial w}{\partial \eta} \right)^2 + \frac{k^v_{\eta=-1}}{b} (w)^2 \right]_{\eta=-1} \mathrm{d}\xi. \end{aligned} \tag{32}$$

By substituting Equation (8) into Equation (32), we obtain:

$$\begin{aligned} U_{mag} &= U_{mag}^{I} + U_{mag}^{III} \\ &= \frac{ab}{2}\int_{-1}^{1}\left[\frac{D_{11}}{a^4}J_4\psi^2 + \frac{2D_{12}}{a^2b^2}J_2\frac{\mathrm{d}^2\psi}{\mathrm{d}\eta^2}\psi + \frac{D_{22}}{b^4}J_1\left(\frac{\mathrm{d}^2\psi}{\mathrm{d}\eta^2}\right)^2 \right. \\ &\quad \left. + \frac{4D_{66}}{a^2b^2}J_3\left(\frac{\mathrm{d}\psi}{\mathrm{d}\eta}\right)^2\right]\mathrm{d}\eta + abJ_1\left[\frac{k_{\eta=1}^{r}}{b^3}\left(\frac{\mathrm{d}\psi}{\mathrm{d}\eta}\right)^2 + \frac{k_{\eta=1}^{v}}{b}\left(\psi\right)^2\right]_{\eta=1} \\ &\quad + abJ_1\left[\frac{k_{\eta=-1}^{r}}{b^3}\left(\frac{\mathrm{d}\psi}{\mathrm{d}\eta}\right)^2 + \frac{k_{\eta=-1}^{v}}{b}\left(\psi\right)^2\right]_{\eta=-1}, \end{aligned} \tag{33}$$

where the integral parameters are defined as:

$$\begin{aligned} J_1 &= \int_{-1}^{1}\phi^2\,\mathrm{d}\xi, \\ J_2 &= \int_{-1}^{1}\left(\frac{\mathrm{d}^2\phi}{\mathrm{d}\xi^2}\phi\right)\mathrm{d}\xi, \\ J_3 &= \int_{-1}^{1}\left(\frac{\mathrm{d}\phi}{\mathrm{d}\xi}\right)^2\mathrm{d}\xi, \\ J_4 &= \int_{-1}^{1}\left(\frac{\mathrm{d}^2\phi}{\mathrm{d}\xi^2}\right)^2\mathrm{d}\xi. \end{aligned} \tag{34}$$

The coefficient T_0 of the kinetic energy from Equation (7) for the plate can be expressed as:

$$T_0 = \frac{ab}{2}\rho h J_1\int_{-1}^{1}\psi^2\,\mathrm{d}\eta. \tag{35}$$

Take the Rayleigh principle in the form:

$$\delta U_{mag} = \omega_y^2\,\delta T_0. \tag{36}$$

By substituting Equations (33) and (35) into Equation (36), and relieving

$\delta\psi$ and $\delta\frac{\mathrm{d}\psi}{\mathrm{d}\eta}$ in Equation (36) by variation calculus, yields:

$$\begin{aligned}
0 = &\int_{-1}^{1}\left[\frac{D_{22}}{b^4}J_1\frac{d^4\psi}{\mathrm{d}\eta^4} + \left(\frac{2D_{12}}{a^2b^2}J_2 - \frac{4D_{66}}{a^2b^2}J_3\right)\frac{\mathrm{d}^2\psi}{\mathrm{d}\eta^2}\right.\\
&\left.+\left(\frac{D_{11}}{a^4}J_4 - \omega_y^2\rho h J_1\right)\psi\right]\delta\psi\,\mathrm{d}\eta\\
&+\frac{2k^v_{\eta=-1}}{b}J_1(\psi\delta\psi)_{\eta=-1} + \frac{2k^v_{\eta=1}}{b}J_1(\psi\delta\psi)_{\eta=1}\\
&+\left[\left(\frac{4D_{66}}{a^2b^2}J_3 - \frac{D_{12}}{a^2b^2}J_2\right)\frac{\mathrm{d}\psi}{\mathrm{d}\eta} - \frac{D_{22}}{b^4}J_1\frac{\mathrm{d}^3\psi}{\mathrm{d}\eta^3}\right]\delta\psi\Big|_{\eta=-1}^{\eta=1}\\
&+\left(\frac{D_{12}}{a^2b^2}J_2\psi + \frac{D_{22}}{b^4}J_1\frac{\mathrm{d}^2\psi}{\mathrm{d}\eta^2}\right)\delta\frac{\mathrm{d}\psi}{\mathrm{d}\eta}\Big|_{\eta=-1}^{\eta=1}\\
&+\frac{2k^r_{\eta=-1}}{b^3}J_1\left(\frac{\mathrm{d}\psi}{\mathrm{d}\eta}\delta\frac{\mathrm{d}\psi}{\mathrm{d}\eta}\right)_{\eta=-1} + \frac{2k^r_{\eta=1}}{b^3}J_1\left(\frac{\mathrm{d}\psi}{\mathrm{d}\eta}\delta\frac{\mathrm{d}\psi}{\mathrm{d}\eta}\right)_{\eta=1}.
\end{aligned}\tag{37}$$

Thus, the governing differential equation in the y-direction can be obtained from the integration part in Equation (37):

$$\frac{\mathrm{d}^4\psi}{\mathrm{d}\eta^4} + \frac{2}{\alpha^2}\left(\frac{D_{12}J_2}{D_{22}J_1} - 2\frac{D_{66}J_3}{D_{22}J_1}\right)\frac{\mathrm{d}^2\psi}{\mathrm{d}\eta^2} + \left(\frac{D_{11}J_4}{\alpha^4D_{22}J_1} - \frac{b^4D_{11}}{D_{22}}\Omega_y^4\right)\psi = 0, \tag{38}$$

where $\Omega_y = \sqrt[4]{\omega_y^2\rho h/D_{11}}$. By substituting $\psi(\eta) = Be^{\lambda\eta}$ into Equation (38), yields:

$$\lambda^4 + \frac{2}{\alpha^2}\left(\frac{D_{12}J_2}{D_{22}J_1} - 2\frac{D_{66}J_3}{D_{22}J_1}\right)\lambda^2 + \left(\frac{D_{11}J_4}{\alpha^4D_{22}J_1} - \frac{b^4D_{11}}{D_{22}}\Omega_y^4\right) = 0. \tag{39}$$

The solution for λ can be expressed as:

$$\lambda_{1,2} = \pm i\alpha_2, \qquad \lambda_{3,4} = \pm\beta_2, \tag{40}$$

where,

$$\alpha_2 = \frac{1}{\alpha}\sqrt{\sqrt{\left(\frac{D_{12}J_2}{D_{22}J_1} - 2\frac{D_{66}J_3}{D_{22}J_1}\right)^2 - \frac{D_{11}J_4}{D_{22}J_1} + \frac{a^4D_{11}}{D_{22}}\Omega_y^4} + \frac{D_{12}J_2}{D_{22}J_1} - 2\frac{D_{66}J_3}{D_{22}J_1}}, \tag{41a}$$

$$\beta_2 = \frac{1}{\alpha}\sqrt{\sqrt{\left(\frac{D_{12}J_2}{D_{22}J_1} - 2\frac{D_{66}J_3}{D_{22}J_1}\right)^2 - \frac{D_{11}J_4}{D_{22}J_1} + \frac{a^4D_{11}}{D_{22}}\Omega_y^4} - \frac{D_{12}J_2}{D_{22}J_1} + 2\frac{D_{66}J_3}{D_{22}J_1}}. \tag{41b}$$

The boundary conditions along the edges in the y-direction can be obtained from the remaining $\delta\psi$ and $\delta\frac{\mathrm{d}\psi}{\mathrm{d}\eta}$ parts in Equation (37). The shear force equilibrium can be obtained from the $\delta\psi$ part:

$$\begin{aligned}&\left[\left(\frac{4D_{66}}{a^2b^2}J_3-\frac{D_{12}}{a^2b^2}J_2\right)\frac{\mathrm{d}\psi}{\mathrm{d}\eta}-\frac{D_{22}}{b^4}J_1\frac{\mathrm{d}^3\psi}{\mathrm{d}\eta^3}\right]\Bigg|_{\eta=-1}^{\eta=1}\\&+\frac{2k^v_{\eta=-1}}{b}J_1(\psi)_{\eta=-1}+\frac{2k^v_{\eta=1}}{b}J_1(\psi)_{\eta=1}=0,\end{aligned}\tag{42}$$

and from the $\delta\frac{\mathrm{d}\psi}{\mathrm{d}\eta}$ part, the bending moment equilibrium:

$$\begin{aligned}&\left(\frac{D_{12}}{a^2b^2}J_2\psi+\frac{D_{22}}{b^4}J_1\frac{\mathrm{d}^2\psi}{\mathrm{d}\eta^2}\right)\Bigg|_{\eta=-1}^{\eta=1}+\frac{2k^r_{\eta=-1}}{b^3}J_1\left(\frac{\mathrm{d}\psi}{\mathrm{d}\eta}\right)_{\eta=-1}\\&\qquad+\frac{2k^r_{\eta=1}}{b^3}J_1\left(\frac{\mathrm{d}\psi}{\mathrm{d}\eta}\right)_{\eta=1}=0.\end{aligned}\tag{43}$$

Thus, we can obtain the shear force and bending moment equilibrium along the edges $\eta=-1$ and $\eta=1$ from Equations (42) and (43), respectively, as:

$$\frac{\mathrm{d}^3\psi}{\mathrm{d}\eta^3}-\left(\frac{4D_{66}J_3}{\alpha^2D_{22}J_1}-\frac{D_{12}J_2}{\alpha^2D_{22}J_1}\right)\frac{\mathrm{d}\psi}{\mathrm{d}\eta}+\frac{2b^3k^v_{\eta=-1}}{D_{22}}\psi=0,\qquad \eta=-1,\tag{44a}$$

$$\frac{\mathrm{d}^2\psi}{\mathrm{d}\eta^2}+\frac{D_{12}J_2}{\alpha^2D_{22}J_1}\psi-\frac{2bk^r_{\eta=-1}}{D_{22}}\frac{\mathrm{d}\psi}{\mathrm{d}\eta}=0,\qquad \eta=-1,\tag{44b}$$

$$\frac{\mathrm{d}^3\psi}{\mathrm{d}\eta^3}-\left(\frac{4D_{66}J_3}{\alpha^2D_{22}J_1}-\frac{D_{12}J_2}{\alpha^2D_{22}J_1}\right)\frac{\mathrm{d}\psi}{\mathrm{d}\eta}-\frac{2b^3k^v_{\eta=1}}{D_{22}}\psi=0,\qquad \eta=1,\tag{44c}$$

$$\frac{\mathrm{d}^2\psi}{\mathrm{d}\eta^2}+\frac{D_{12}J_2}{\alpha^2D_{22}J_1}\psi+\frac{2bk^r_{\eta=1}}{D_{22}}\frac{\mathrm{d}\psi}{\mathrm{d}\eta}=0,\qquad \eta=1.\tag{44d}$$

Substituting Equation (9b) into Equation (44) and denoting $k^{v*}_\eta=\frac{2b^3k^v_\eta}{D_{22}}$, $k^{r*}_\eta=\frac{2bk^r_\eta}{D_{22}}$, $S_{\alpha_2}=\sin\alpha_2$, $C_{\alpha_2}=\cos\alpha_2$, $Sh_{\alpha_2}=\sinh\alpha_2$, $Ch_{\alpha_2}=\cosh\alpha_2$, $S_{\beta_2}=\sin\beta_2$, $C_{\beta_2}=\cos\beta_2$, $Sh_{\beta_2}=\sinh\beta_2$, and $Ch_{\beta_2}=\cosh\beta_2$, We obtain:

$$\begin{bmatrix}\zeta_1C_{\alpha_2}-k^{v*}_{\eta=-1}S_{\alpha_2} & \zeta_1S_{\alpha_2}+k^{v*}_{\eta=-1}C_{\alpha_2} & \zeta_2Ch_{\beta_2}-k^{v*}_{\eta=-1}Sh_{\beta_2} & -\zeta_2Sh_{\beta_2}+k^{v*}_{\eta=-1}Ch_{\beta_2}\\ \zeta_3S_{\alpha_2}+k^{r*}_{\eta=-1}\alpha_2C_{\alpha_2} & -\zeta_3C_{\alpha_2}+k^{r*}_{\eta=-1}\alpha_2S_{\alpha_2} & \zeta_4Sh_{\beta_2}+k^{r*}_{\eta=-1}\beta_2Ch_{\beta_2} & -\zeta_4Ch_{\beta_2}-k^{r*}_{\eta=-1}\beta_2Sh_{\beta_2}\\ -\zeta_1C_{\alpha_2}+k^{v*}_{\eta=1}S_{\alpha_2} & \zeta_1S_{\alpha_2}+k^{v*}_{\eta=1}C_{\alpha_2} & -\zeta_2Ch_{\beta_2}+k^{v*}_{\eta=1}Sh_{\beta_2} & -\zeta_2Sh_{\beta_2}+k^{v*}_{\eta=1}Ch_{\beta_2}\\ \zeta_3S_{\alpha_2}+k^{r*}_{\eta=1}\alpha_2C_{\alpha_2} & \zeta_3C_{\alpha_2}-k^{r*}_{\eta=1}\alpha_2S_{\alpha_2} & \zeta_4Sh_{\beta_2}+k^{r*}_{\eta=1}\beta_2Ch_{\beta_2} & \zeta_4Ch_{\beta_2}+k^{r*}_{\eta=1}\beta_2Sh_{\beta_2}\end{bmatrix}\begin{Bmatrix}B_1\\B_2\\B_3\\B_4\end{Bmatrix}=\begin{Bmatrix}0\\0\\0\\0\end{Bmatrix},\tag{45}$$

or,

$$\mathbf{R}_y \mathbf{B} = \mathbf{0}, \tag{46}$$

where,

$$\begin{aligned}
\zeta_1 &= -\alpha_2^3 - \left(\frac{4D_{66}J_3}{\alpha^2 D_{22} J_1} - \frac{D_{12}J_2}{\alpha^2 D_{22} J_1}\right)\alpha_2, \\
\zeta_2 &= \beta_2^3 - \left(\frac{4D_{66}T_3}{\alpha^2 D_{22} J_1} - \frac{D_{12}J_2}{\alpha^2 D_{22} J_1}\right)\beta_2, \\
\zeta_3 &= -\alpha_2^2 + \frac{D_{12}J_2}{\alpha^2 D_{22} J_1}, \\
\zeta_4 &= \beta_2^2 + \frac{D_{12}J_2}{\alpha^2 D_{22} J_1}.
\end{aligned} \tag{47}$$

With the help of Equation (9b), the vertical displacement and rotation corresponding to the mode shape ψ along the y-direction at the edges $\eta = -1$ and $\eta = 1$ can be expressed as:

$$\begin{Bmatrix} \psi_{\eta=-1} \\ \frac{\mathrm{d}\psi}{\mathrm{d}\eta}_{\eta=-1} \\ \psi_{\eta=1} \\ \frac{\mathrm{d}\psi}{\mathrm{d}\eta}_{\eta=1} \end{Bmatrix} = \begin{bmatrix} -S_{\alpha_2} & C_{\alpha_2} & -Sh_{\beta_2} & Ch_{\beta_2} \\ \frac{\alpha_2 C_{\alpha_2}}{b} & \frac{\alpha_2 S_{\alpha_2}}{b} & \frac{\beta_2 Ch_{\beta_2}}{b} & -\frac{\beta_2 Sh_{\beta_2}}{b} \\ S_{\alpha_2} & C_{\alpha_2} & Sh_{\beta_2} & Ch_{\beta_2} \\ \frac{\alpha_2 C_{\alpha_2}}{b} & -\frac{\alpha_2 S_{\alpha_2}}{b} & \frac{\beta_2 Ch_{\beta_2}}{b} & \frac{\beta_2 Sh_{\beta_2}}{b} \end{bmatrix} \begin{Bmatrix} B_1 \\ B_2 \\ B_3 \\ B_4 \end{Bmatrix}, \tag{48}$$

or,

$$\delta_y = \mathbf{Q}_y \mathbf{B}. \tag{49}$$

Note that the eigenvector $\mathbf{B}$ can be expressed by multiplying the inverse matrix $\mathbf{Q}_y^{-1}$ on the left-hand side of Equation (49), and then substituting $\mathbf{B}$ into Equation (46), we obtain:

$$\mathbf{R}_y \mathbf{B} = \mathbf{R}_y \mathbf{Q}_x^{-1} \delta_y = \mathbf{0}, \tag{50}$$

where the dynamic stiffness matrix, denoted as $\mathbf{K}_y = \mathbf{R}_y \mathbf{Q}_y^{-1}$, can be obtained from Equation (50).

3. Frequency and mode shape computation

3.1. Wittrick–Williams algorithm and enhancement

The Wittrick–Williams (W-W) algorithm [23] is an effective method for determining the natural frequencies from the dynamic stiffness matrix with high reliability. Instead of directly solving the equations, the algorithm computes the total number J of natural frequencies below a given frequency ω^*, which is represented as:

$$J(\omega^*) = J_0(\omega^*) + s\{\mathbf{K}^{\Delta}(\omega^*)\} = J_0(\omega^*) + J_k(\omega^*), \tag{51}$$

where J_0 represents the number of natural frequencies for the system with both ends fully clamped, $\mathbf{K}^{\Delta}$ is the upper triangular matrix obtained from the dynamic stiffness matrix $\mathbf{K}$ after applying Gaussian elimination, and $J_k(\omega^*)$ denotes the number of negative elements in the leading diagonal of $\mathbf{K}^{\Delta}$.

It should be noted that the J_0 count is a crucial aspect when applying the W-W algorithm. Many previous studies use a sufficiently fine mesh or enough terms in series expansions to capture all fully clamped natural frequencies, ensuring computational accuracy [1]. However, this approach can make the application process cumbersome. To address this issue, the fully clamped problem can be replaced with a simply supported problem, where the Navier solution for the simply supported plate is used to count J_0 [18]. Nevertheless, since analytical solutions in DSM methods involve an infinite series of Fourier terms, a sufficient number of truncation terms is required to ensure accuracy and convergence.

However, the idea of solving the simply supported problem proposes an effective and systematic approach to indirectly determine the J_0 count for a fully clamped structure, where the boundary conditions are modeled as pinned supports rather than clamped ones [8]:

$$J_0(p_1, \omega^*) = J(\bar{p}_1, \omega^*) - J_k(\bar{p}_1, \omega^*), \tag{52}$$

where p_1 and $\bar{p}_1$ represent clamped and pinned supports, respectively. By substituting Equation (52) into Equation (51) we get the algorithm as:

$$J(p, \omega^*) = J(\bar{p}_1, \omega^*) - J_k(\bar{p}_1, \omega^*) + J_k(p, \omega^*) \tag{53}$$

where p represents the original boundary conditions of the structure. Therefore, the challenge of determining $J_0(p_1, \omega^*)$ can be transformed into the problem of solving $J(\bar{p}_1, \omega^*)$ instead. The eigenvalue equation corresponding to the natural frequency parameter Ω_x can be obtained from the determinant of the coefficient matrix $\mathbf{R}_x$ in Equation (25), which is given by [27]:

$$\sin 2\alpha_1 = 0. \tag{54}$$

With the help of Equations (21a) and (54), the closed-form solution of the n_xth simply supported frequency Ω_{x,n_x} for the given n_y-order $\psi_{n_y}(\eta)$ can be expressed as:

$$\Omega_{x,n_x} = \frac{1}{b}\sqrt[4]{\left[\left(\frac{n_x\pi}{2\alpha}\right)^2 - \frac{D_{12}S_2}{D_{11}S_1} + 2\frac{D_{66}S_3}{D_{11}S_1}\right]^2 - \left(\frac{D_{12}S_2}{D_{11}S_1} - 2\frac{D_{66}S_3}{D_{11}S_1}\right)^2 + \frac{D_{22}S_4}{D_{11}S_1}}. \tag{55}$$

For $\Omega_{x,n_x} \leq \Omega_x^* < \Omega_{x,n_{x+1}}$, $J(\bar{p}_1, \Omega_x^*) = n_x$. Similarly, the closed-form solution of the n_y-th simply supported frequency Ω_{y,n_y} for the given n_x-order $\phi_{n_x}(\xi)$ can be expressed as:

$$\Omega_{y,n_y} = \frac{1}{a}\sqrt[4]{\frac{D_{22}}{D_{11}}\left\{\left[\left(\frac{n_y\pi\alpha}{2}\right)^2 - \frac{D_{12}T_2}{D_{22}T_1} + 2\frac{D_{66}T_3}{D_{22}T_1}\right]^2 - \left(\frac{D_{12}T_2}{D_{22}T_1} - 2\frac{D_{66}T_3}{D_{22}T_1}\right)^2 + \frac{D_{11}T_4}{D_{22}T_1}\right\}}. \tag{56}$$

For $\Omega_{y,n_y} \leq \Omega_y^* < \Omega_{y,n_{y+1}}$, $J(\bar{p}_1, \Omega_y^*) = n_y$. According to the relationships $\Omega_x = \sqrt[4]{\omega_x^2\rho h/D_{11}}$ and $\Omega_y = \sqrt[4]{\omega_y^2\rho h/D_{11}}$, the values of $J(\bar{p}_1, \omega_x^*)$ and $J(\bar{p}_1, \omega_y^*)$ can be derived from $J(\bar{p}_1, \Omega_x^*)$ and $J(\bar{p}_1, \Omega_y^*)$, respectively. Therefore, this refined W-W algorithm can be applied to estimate the lower and upper bounds of the frequency range, denoted as ω_l and ω_u, yielding an approximation for the frequency $\omega_a \in (\omega_l, \omega_u)$.

3.2. Mode shape computation

The mode shape coefficients A_1 to A_4 and B_1 to B_4 in the eigenvectors $\mathbf{A}$ and $\mathbf{B}$ for all classic boundary conditions are provided in [27]. Alternatively, these coefficients can also be obtained through a simple numerical method, which this work presents as an approach. Here, we illustrate solving the eigenvector $\mathbf{A}$ as an example. By assuming the exact natural frequency as ω_k, we can expand the coefficient matrix $\mathbf{R}_x$ in Equation (25) using a first-order Taylor series about ω_a:

$$\mathbf{R}_{x,k}(\omega_k)\mathbf{A}_k = \mathbf{R}_{x,a}\mathbf{A}_k + (\omega_k - \omega_a)\mathbf{R}'_{x,a}\mathbf{A}_k + O\left((\omega_k - \omega_a)^2\right) = 0. \tag{57}$$

Ignoring higher-order terms, an eigenvalue problem can be derived from Equation (57):

$$(\mathbf{R}'_{x,a})^{-1}\mathbf{R}_{x,a}\mathbf{A} = (\omega_a - \omega_k)\mathbf{A} = \tau\mathbf{A}. \tag{58}$$

This eigenvalue problem can be solved using the inverse iteration procedure [30]:

$$\bar{\mathbf{A}}^{(i+1)} = \mathbf{R}_{x,a}^{-1}\mathbf{R}_{x,a}^{'}\mathbf{A}^{(i)}, \tag{59}$$

where the initial guess for $\mathbf{A}^{(0)}$ is a column vector consisting of four randomly generated elements, each of which falls within the range (0,1). The updated eigenvalue for the next step can be obtained as:

$$\tau^{(i+1)} = \frac{1}{\bar{A}_j^{(i+1)}}, \tag{60}$$

where,

$$\mid \bar{A}_j^{(i+1)} \mid = \max(\mid \bar{A}_1^{(i+1)} \mid, \mid \bar{A}_2^{(i+1)} \mid, \mid \bar{A}_3^{(i+1)} \mid, \mid \bar{A}_4^{(i+1)} \mid). \tag{61}$$

The updated eigenvector can be obtained as:

$$\mathbf{A}^{(i+1)} = \tau^{(i+1)}\bar{\mathbf{A}}^{(i+1)}. \tag{62}$$

The procedure can be controlled by the error tolerance ϵ or maximum allowed steps $i_{\max}$:

$$\max \mid A_n^{(i+1)} - A_n^{(i)} \mid < \epsilon, \tag{63a}$$

$$i = i_{\max}. \tag{63b}$$

Note that the mode shape coefficients A_1 to A_4 obtained from $\mathbf{A}^{(i+1)}$ are applied for the elastically restrained boundary conditions.

3.3. Application procedure

The procedure of the proposed method is as follows:

- **Step 1** Assume initial integral parameters $I_1^{(0)}, I_2^{(0)}, I_3^{(0)}$, and $I_4^{(0)}$ in the y-direction. Using the given boundary conditions at $\xi = -1$ and $\xi = 1$, determine $\mathbf{K}_x^{(0)}$ from Equation (30). Then, apply the computational algorithms in Section 3.1 to compute the lower and upper bounds of the n_x-th non-dimensional frequency parameter, $2a\Omega_{l,x,n_x}^{(0)}$ and $2a\Omega_{u,x,n_x}^{(0)}$, and take the average $2a\Omega_{x,n_x}^{(0)} = (2a\Omega_{l,x,n_x}^{(0)} + 2a\Omega_{u,x,n_x}^{(0)})/2$ along with its corresponding mode shape $\phi_{n_x}^{(0)}$, where $n_x = 1, 2, 3, \ldots$.

- **Step 2** Use $\phi_{n_x}^{(0)}$ as the prescribed mode to determine $\mathbf{K}_y^{(1)}$ in Equation (50), considering the boundary conditions at $\eta = -1$ and $\eta = 1$. Apply the computational algorithms to obtain the n_y-th frequency parameter $2a\Omega_{y,n_y}^{(1)}$ and its corresponding mode shape $\psi_{n_y}^{(1)}$, where $n_y = 1, 2, 3, \ldots$. This completes the first iteration cycle.

- **Step 3** Use $\psi_{n_y}^{(1)}$ as the prescribed n_y-th mode shape in the y-direction to compute $\mathbf{K}_x^{(1)}$ from Equation (30), then determine the n_x-th frequency parameter $2a\Omega_{x,n_x}^{(1)}$ and its corresponding mode shape $\phi_{n_x}^{(1)}$.

- **Step 4** Use $\phi_{n_x}^{(1)}$ as the prescribed mode in the x-direction to compute the n_y-th frequency parameter $2a\Omega_{y,n_y}^{(2)}$ and its corresponding mode shape $\psi_{n_y}^{(2)}$, completing the second iteration cycle.

- **Step 5** Stop the iteration if $|2a\Omega_{x,n_x}^{(i)} - 2a\Omega_{x,n_x}^{(i+1)}| \le \Delta 2a\Omega$ or $|2a\Omega_{y,n_y}^{(i)} - 2a\Omega_{y,n_y}^{(i+1)}| \le \Delta 2a\Omega$, where $\Delta 2a\Omega = 2a\Omega_u - 2a\Omega_l$. Here, $2a\Omega_l$ and $2a\Omega_u$ are the lower and upper bounds of the frequency parameter range, within which the actual frequency parameter $2a\Omega$ lies, i.e., $2a\Omega \in (2a\Omega_l, 2a\Omega_u)$. The quantity $\Delta 2a\Omega$ represents the frequency parameter interval used in the W-W algorithm.

- **Step 6** Finally, construct the (n_x, n_y)-th mode shape as $w(\xi, \eta) = \phi_{n_x}(\xi)\psi_{n_y}(\eta)$ using Equation (8).

4. Numerical Results

This section presents the numerical validation of the proposed method for classic boundary conditions and rotationally restrained boundary conditions. For all numerical calculations, the initial integral parameters are assumed as $I_1^{(0)} = 1$, $I_2^{(0)} = 1$, $I_3^{(0)} = 1$, and $I_4^{(0)} = 10$ in the y-direction, serving as the starting point of **Step 1** for any mode in all boundary conditions. In this section, the interval between the upper and lower bounds of the non-dimensional frequency parameter, $2a\Delta\Omega$, is set to 0.005, limiting the error range. According to our numerical calculations, two iteration cycles are generally sufficient to meet the convergence requirement (i.e., $|2a\Omega_x^{(i)} - 2a\Omega_x^{(i+1)}| \le \Delta 2a\Omega$ or $|2a\Omega_y^{(i)} - 2a\Omega_y^{(i+1)}| \le \Delta 2a\Omega$) for most cases, with at most three cycles required when applying the iterative procedure in Section 3.3.

4.1. Classical boundary conditions

In this subsection, the proposed method is validated by comparison with the extended SOV method [27]. The properties of the orthotropic plate, consistent with those in [27], are as follows: $E_1 = 185\text{GPa}$, $E_2 = 10.5\text{GPa}$, $G_{12} = 7.3\text{GPa}$, $\rho = 1600\ \mathrm{kg\,m^{-1}}$, and $\nu_{12} = 0.28$.

The translational springs (k_ξ^v) and rotational springs (k_ξ^r) along all edges can be set to zero or infinity (represented as $1 \times 10^{15}\ \mathrm{N\,m^{-1}}$ in the numerical calculations of this study) to obtain different classic boundary conditions.

The results for SSSS, SCSF, GCGC, CCCC, SSCC, SCCC, GGCC, CCFF, CFCF, CFFF, and FFFF boundary conditions are presented in Tables 1 to 3. These results demonstrate high accuracy compared to the extended SOV method, with difference remaining smaller than the frequency parameter interval $2a\Delta\Omega = 0.005$. The frequency parameters in both directions are equal ($2a\Omega_x - 2a\Omega_y = 0$) in almost all cases, with a few exceptions where $2a\Omega_x - 2a\Omega_y = 0.005$. In fact, higher accuracy compared to the extended SOV method can be achieved if the frequency parameter interval $2a\Delta\Omega$ is set smaller than 0.005. It should be noted that the accuracy improves only by reducing $2a\Delta\Omega$, and no additional iterations are required according to our calculations. Figure 2 shows the first six nonzero mode shapes of a square orthotropic plate with FFFF boundary conditions, where the mode shape coefficients are calculated using the numerical method developed in this study. Instead of selecting fixed expressions for the mode shape coefficients based on specific boundary conditions, our method is applicable to all boundary conditions.

4.2. Rotationally restrained boundary conditions

In this subsection, rectangular orthotropic plates with rotationally restrained edges ($k_\xi^v = k_\eta^v = \infty$) are validated. The rotational stiffness coefficients are defined as:

$$r_\xi = \frac{2ak_\xi^r}{D_{11}}, \tag{64a}$$

$$r_\eta = \frac{2bk_\eta^r}{D_{22}}. \tag{64b}$$

The first example considers a square isotropic plate with all four edges rotationally restrained. The vertical translational springs along the four edges are numerically set as $k_{\xi=-1}^v = k_{\xi=1}^v = k_{\eta=-1}^v = k_{\eta=1}^v = 1 \times 10^{12}\ \mathrm{N\,m^{-1}}$. The material properties are given as $D_{11} = D_{22} = D_3$ and $v_{12} = v_{21} = 0.3$.

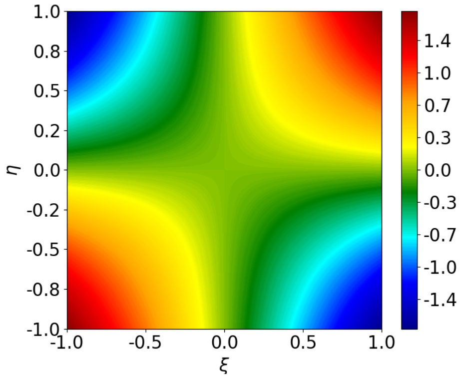

(a)

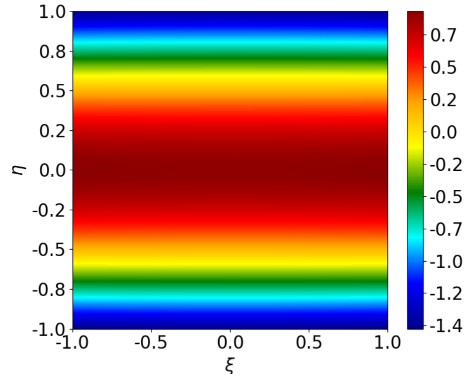

(b)

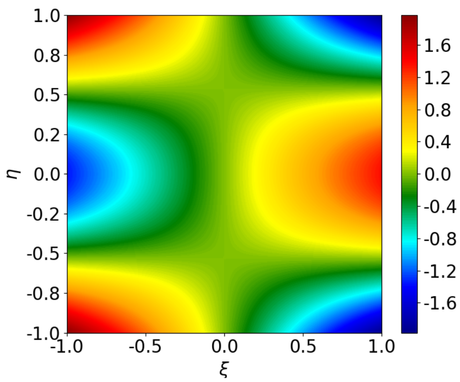

(c)

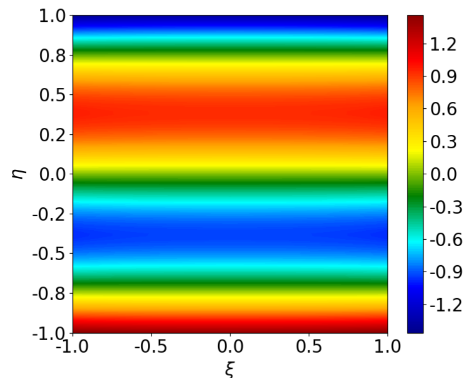

(d)

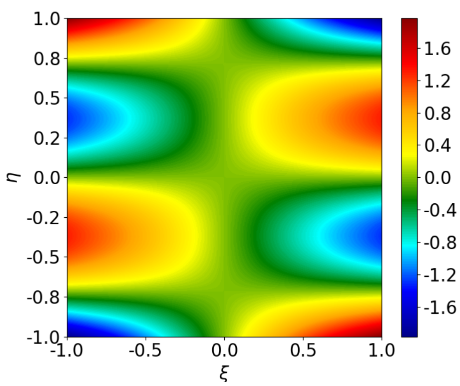

(e)

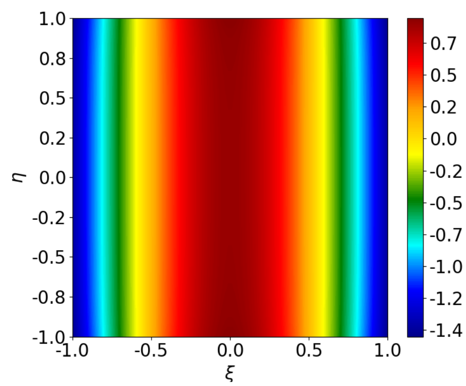

(f)

Figure 2: The first six nonzero mode shapes of a square orthotropic plate with FFFF boundary conditions: (a) the first mode; (b) the second mode; (c) the third mode; (d) the fourth mode; (e) the fifth mode; (f) the sixth mode.

Table 1: The first seven frequency parameter $2a\Omega$ of of orthotropic rectangular plates with SSSS, SCSF and GCGC boundary conditions.

			$2a\Omega_x = 2a\Omega_y = 2a\sqrt[4]{\rho h\omega^2/D_{11}}$						
BCs	α	Mode	1	2	3	4	5	6	7
SSSS	0.5	Mode number	(1,1)	(1,2)	(1,3)	(1,4)	(1,5)	(1,6)	(1,7)
		extended SOV 27	3.1807	3.3190	3.5938	4.0135	4.5495	5.1635	5.8265
		Present	3.1825	3.3225	3.5975	4.0175	4.5525	5.1625	5.8275
	1	Mode number	(1,1)	(1,2)	(1,3)	(2,1)	(1,4)	(2,2)	(2,3)
		extended SOV 27	3.3190	4.0135	5.1635	6.3615	6.5200	6.6379	7.1876
		Present	3.3175	4.0175	5.1625	6.3625	6.5175	6.6375	7.1875
	1.5	Mode number	(1,1)	(1,2)	(2,1)	(2,2)	(1,3)	(2,3)	(1,4)
		extended SOV 27	3.5938	5.1635	6.4698	7.1876	7.2331	8.5389	9.4352
		Present	3.5975	5.1675	6.4725	7.1875	7.2325	8.5375	9.4375
SCSF	0.5	Mode number	(1,1)	(1,2)	(1,3)	(1,4)	(1,5)	(1,6)	(1,7)
		extended SOV 27	3.1516	3.2451	3.4588	3.8131	4.2950	4.8711	5.5087
		Present	3.1525	3.2475	3.4575	3.8175	4.2925	4.8725	5.5075
	1	Mode number	(1,1)	(1,2)	(1,3)	(1,4)	(2,1)	(2,2)	(2,3)
		extended SOV 27	3.1908	3.6428	4.5972	5.8599	6.3033	6.4901	6.9177
		Present	3.1925	3.6425	4.5975	5.8575	6.3025	6.4925	6.9175
	1.5	Mode number	(1,1)	(1,2)	(1,3)	(2,1)	(2,2)	(2,3)	(1,4)
		extended SOV 27	3.2710	4.3430	6.2157	6.3337	6.8043	7.8718	8.3518
		Present	3.2725	4.3425	6.2175	6.3325	6.8025	7.8725	8.3525
GCGC	0.5	Mode number	(1,1)	(1,2)	(1,3)	(2,1)	(2,2)	(1,4)	(2,3)
		extended SOV 27	1.1544	1.9166	2.6835	3.1983	3.3890	3.4501	3.7372
		Present	1.1525	1.9175	2.6825	3.1975	3.3875	3.4525	3.7375
	1	Mode number	(1,1)	(2,1)	(1,2)	(2,2)	(1,3)	(2,3)	(3,1)
		extended SOV 27	2.3087	3.4900	3.8331	4.4682	5.3669	5.7736	6.3967
		Present	2.3075	3.4875	3.8325	4.4675	5.3675	5.7725	6.3975
	1.5	Mode number	(1,1)	(2,1)	(1,2)	(2,2)	(3,1)	(3,2)	(1,3)
		extended SOV 27	3.4631	4.1353	5.7497	6.0981	6.6049	7.6449	8.0504
		Present	3.4625	4.1325	5.7475	6.0975	6.6075	7.6425	8.0525

Table 2: The first seven frequency parameter $2a\Omega$ of of orthotropic rectangular plates with CCCC, SSCC, SCCC and GGCC boundary conditions.

			$2a\Omega_x = 2a\Omega_y = 2a\sqrt[4]{\rho h\omega^2/D_{11}}$						
BCs	α	Mode	1	2	3	4	5	6	7
CCCC	0.5	Mode number	(1,1)	(1,2)	(1,3)	(1,4)	(1,5)	(1,6)	(1,7)
		extended SOV 27	4.7500	4.8208	4.9682	5.2177	5.5791	6.0430	6.5892
		Present	4.7475	4.8225	4.9725	5.2175	5.5825	6.0425	6.5875
	1	Mode number	(1,1)	(1,2)	(1,3)	(1,4)	(2,1)	(2,2)	(2,3)
		extended SOV 27	4.8579	5.3546	6.2819	7.4972	7.9193	8.1490	8.6054
		Present	4.8575	5.3575	6.2875	7.4975	7.9175	8.1475	8.6075
	1.5	Mode number	(1,1)	(1,2)	(2,1)	(1,3)	(2,2)	(2,3)	(1,4)
		extended SOV 27	5.1581	6.5412	8.0409	8.4945	8.7204	9.9793	10.6460
		Present	5.1575	6.5375	8.0425	8.4975	8.7175	9.9775	10.6425
SSCC	0.5	Mode number	(1,1)	(1,2)	(1,3)	(1,4)	(1,5)	(1,6)	(1,7)
		extended SOV 27	3.9542	4.0520	4.2525	4.5785	5.0254	5.5682	6.1789
		Present	3.9575	4.0525	4.2475	4.5775	5.0225	5.5725	6.1825
	1	Mode number	(1,1)	(1,2)	(1,3)	(1,4)	(2,1)	(2,2)	(2,3)
		extended SOV 27	4.0745	4.6606	5.7009	6.9940	7.1396	7.3894	7.8881
		Present	4.0775	4.6625	5.7025	6.9925	7.1375	7.3875	7.8875
	1.5	Mode number	(1,1)	(1,2)	(2,1)	(1,3)	(2,2)	(2,3)	(1,4)
		extended SOV 27	4.3602	5.8384	7.2531	7.8560	7.9481	9.2515	10.0366
		Present	4.3625	5.8325	7.2525	7.8575	7.9525	9.2525	10.0325
SCCC	0.5	Mode number	(1,1)	(1,2)	(1,3)	(1,4)	(1,5)	(1,6)	(1,7)
		extended SOV 27	3.9596	4.0745	4.3027	4.6606	5.1361	5.7009	6.3271
		Present	3.9575	4.0725	4.3025	4.6625	5.1325	5.7025	6.3325
	1	Mode number	(1,1)	(1,2)	(1,3)	(2,1)	(1,4)	(2,2)	(2,3)
		extended SOV 27	4.1349	4.8478	5.9805	7.1541	7.3192	7.4478	8.0121
		Present	4.1325	4.8475	5.9825	7.1525	7.3175	7.4475	8.0125
	1.5	Mode number	(1,1)	(1,2)	(2,1)	(2,2)	(1,3)	(2,3)	(3,1)
		extended SOV 27	4.5824	6.2766	7.3116	8.1528	8.3705	9.5986	10.3507
		Present	4.5825	6.2775	7.3125	8.1525	8.3725	9.5975	10.3525
GGCC	0.5	Mode number	(1,1)	(1,2)	(1,3)	(1,4)	(1,5)	(1,6)	(1,7)
		extended SOV 27	2.3750	2.4841	2.7895	3.2946	3.9226	4.6123	5.3326
		Present	2.3725	2.4875	2.7925	3.2975	3.9225	4.6075	5.3325
	1	Mode number	(1,1)	(1,2)	(1,3)	(2,1)	(2,2)	(1,4)	(2,3)
		extended SOV 27	2.4290	3.1410	4.4293	5.5202	5.7315	5.8801	6.2606
		Present	2.4325	3.1425	4.4325	5.5225	5.7325	5.8775	6.2625
	1.5	Mode number	(1,1)	(1,2)	(2,1)	(2,2)	(1,3)	(2,3)	(3,1)
		extended SOV 27	2.5790	4.2472	5.5565	6.1533	6.4347	7.5231	8.6732
		Present	2.5825	4.2475	5.5575	6.1525	6.4325	7.5225	8.6725

Table 3: The first seven nonzero frequency parameter $2a\Omega$ of of orthotropic rectangular plates with CCFF, CFCF, CFFF and FFFF boundary conditions.

			$2a\Omega_x = 2a\Omega_y = 2a\sqrt[4]{\rho h\omega^2/D_{11}}$						
BCs	α	Mode	1	2	3	4	5	6	7
CCFF	0.5	Mode number	(1,1)	(1,2)	(1,3)	(1,4)	(1,5)	(1,6)	(2,1)
		extended SOV 27	1.8978	2.0905	2.4925	3.0563	3.7110	4.4117	4.7029
		Present	1.8975	2.0925	2.4925	3.0575	3.7125	4.4125	4.7025
	1	Mode number	(1,1)	(1,2)	(1,3)	(2,1)	(2,2)	(1,4)	(2,3)
		extended SOV 27	1.9930	2.7895	4.0733	4.7338	5.0652	5.5128	5.7419
		Present	1.9925	2.7875	4.0725	4.7325	5.0675	5.5125	5.7425
	1.5	Mode number	(1,1)	(1,2)	(2,1)	(2,2)	(1,3)	(2,3)	(3,1)
		extended SOV 27	2.1780	3.7411	4.7931	5.5758	5.8895	7.0263	7.9006
		Present	2.1775	3.7425	4.7925	5.5725	5.8875	7.0275	7.9025
CFCF	0.5	Mode number	(1,1)	(1,2)	(1,3)	(1,4)	(1,5)	(1,6)	(1,7)
		extended SOV 27	4.7297	4.7427	4.7881	4.8819	5.0478	5.3072	5.6694
		Present	4.7275	4.7425	4.7875	4.8825	5.0475	5.3075	5.6675
	1	Mode number	(1,1)	(1,2)	(1,3)	(1,4)	(1,5)	(1,6)	(2,1)
		extended SOV 27	4.7295	4.7817	5.0012	5.5348	6.4407	7.6182	7.8523
		Present	4.7275	4.7825	5.0025	5.5325	6.4425	7.6175	7.8525
	1.5	Mode number	(1,1)	(1,2)	(1,3)	(1,4)	(2,1)	(2,2)	(2,3)
		extended SOV 27	4.7292	4.8458	5.4221	6.7635	7.8518	7.9470	8.3021
		Present	4.7275	4.8475	5.4225	6.7625	7.8525	7.9475	8.3025
CFFF	0.5	Mode number	(1,1)	(1,2)	(1,3)	(1,4)	(1,5)	(1,6)	(1,7)
		extended SOV 27	1.8751	1.9439	2.1679	2.5657	3.1106	3.7486	4.4382
		Present	1.8775	1.9425	2.1675	2.5675	3.1125	3.7475	4.4375
	1	Mode number	(1,1)	(1,2)	(1,3)	(1,4)	(2,1)	(2,2)	(2,3)
		extended SOV 27	1.8750	2.1242	2.9077	4.1319	4.6937	4.8226	5.2263
		Present	1.8775	2.1225	2.9075	4.1325	4.6925	4.8225	5.2275
	1.5	Mode number	(1,1)	(1,2)	(1,3)	(2,1)	(2,2)	(2,3)	(1,4)
		extended SOV 27	1.8750	2.3402	3.8522	4.6935	4.9753	5.8314	5.9292
		Present	1.8775	2.3425	3.8525	4.6925	4.9775	5.8325	5.9275
FFFF	0.5	Mode number	(1,3)	(2,2)	(1,4)	(2,3)	(1,5)	(2,4)	(2,5)
		extended SOV 27	1.1540	1.4858	1.9157	2.1704	2.6821	2.7881	3.4093
		Present	1.1525	1.4875	1.9175	2.1725	2.6825	2.7875	3.4075
	1	Mode number	(2,2)	(1,3)	(2,3)	(1,4)	(2,4)	(3,1)	(3,2)
		extended SOV 27	2.1311	2.3082	3.2734	3.8320	4.4962	4.7298	4.9138
		Present	2.1325	2.3075	3.2725	3.8325	4.4975	4.7275	4.9125
	1.5	Mode number	(2,2)	(1,3)	(2,3)	(3,1)	(3,2)	(1,4)	(3,3)
		extended SOV 27	2.6277	3.4625	4.2915	4.7296	5.1259	5.7485	6.1588
		Present	2.6275	3.4625	4.2925	4.7275	5.1275	5.7475	6.1575

Table 4 presents the frequency parameter $2a\Omega$ for different rotational stiffness coefficients $r_\xi = r_\eta$ with values $0.1, 1, 10, 100$, and 1000. Notably, when $r_\xi = r_\eta = 0$ and $r_\xi = r_\eta = \infty$, the boundary conditions correspond to SSSS and CCCC, respectively.

Interestingly, the results indicate that the frequencies Ω_x and Ω_y are not strictly equal for some mode shapes under rotationally restrained boundary conditions. The actual frequency Ω lies between Ω_x and Ω_y, which may be attributed to the fact that Ω_x and Ω_y satisfy Rayleigh's principle in Equation (3), representing the weak-form governing equations, but do not necessarily satisfy the strong-form governing equations in Equation (1). For a physical problem with exact solutions, both Equations (1) and (3) must be satisfied. If this condition is not met, applying Equation (3) still provides a viable approach for approximating the exact solution of the plate. Thus, the exact frequency can be estimated as $\Omega = (\Omega_x + \Omega_y)/2$. As shown in Table 4, the maximum difference between Ω and the solutions reported in 31 is less than 1.3%. Figure 3 illustrates the variation in mode shapes corresponding to the fundamental natural frequency as the rotational stiffness $r_\xi = r_\eta$ increases from zero to ∞, transitioning the boundary conditions from SSSS to CCCC.

The next example considers a rectangular orthotropic plate with three simply supported edges ($k^r_{\xi=-1} = k^r_{\xi=1} = k^r_{\eta=1} = 0$), while the edge at $\eta = -1$ is rotationally restrained. The material properties are consistent with those in 31, where $2D_{11} = 2D_{22} = D_3$ and $\nu_{12} = \nu_{21} = 0.3$. Table 5 shows the fundamental frequency results for different length ratios (b/a), comparing them with those reported in 31. The maximum observed difference is 0.8% when $r_{\eta=-1} = 10$.

In certain numerical calculations involving rotationally restrained boundary conditions, the variables α_1 and α_2 may take complex values rather than being purely real. Consequently, the mode shape coefficients A_1, A_2, B_1, and B_2 become complex-valued, leading to $\mathbf{R}$ and $\mathbf{Q}^{-1}$ being complex matrices. However, the mode shapes $\phi(\xi)$ and $\psi(\eta)$ remain real-valued, and the dynamic stiffness matrix $\mathbf{K} = \mathbf{R}\mathbf{Q}^{-1}$ is a real symmetric matrix. Thus, the frequency Ω can be obtained by solving $\mathbf{K}$ using the refined W-W algorithm provided in this study, which avoids solving the eigenvalue equations in both the real and complex domains.

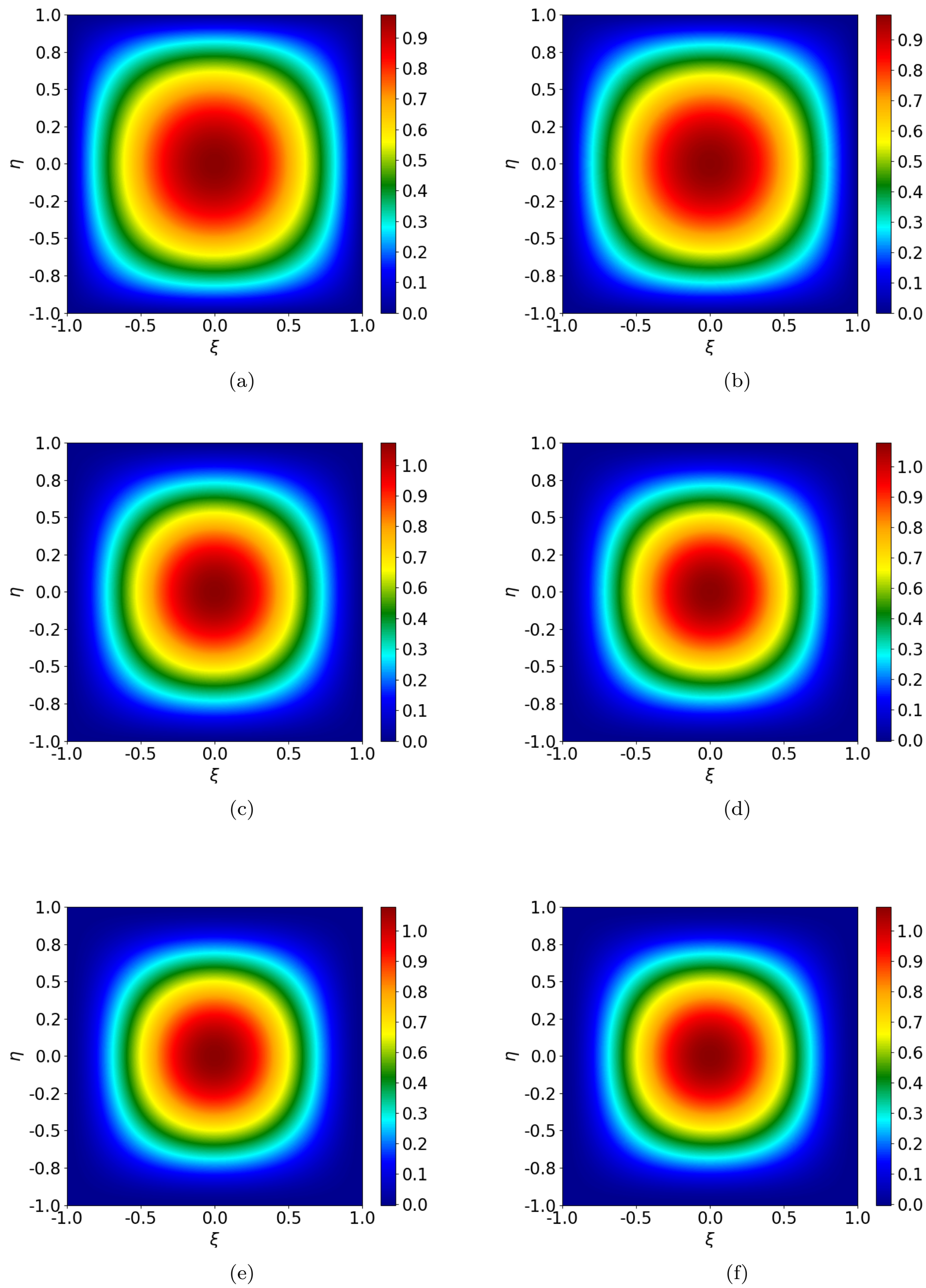

Figure 3: The first mode shape of a square isotropic plate with all four edges rotationally restrained: (a) $r_\xi = r_\eta = 0$; (b) $r_\xi = r_\eta = 1$; (c) $r_\xi = r_\eta = 10$; (d) $r_\xi = r_\eta = 20$; (e) $r_\xi = r_\eta = 100$; (f) $r_\xi = r_\eta = \infty$.

Table 4: The first six frequency parameters, $2a\Omega = 2a\sqrt[4]{\rho h\omega^2/D_{11}}$, of a square isotropic plate with all four edges rotationally restrained, where $k^r_{\xi=-1} = k^r_{\xi=1} = k^r_{\eta=-1} = k^r_{\eta=1}$.

		$2a\Omega$					
r	Mode	1	2	3	4	5	6
0.1	Mode number	(1,1)	(1,2)	(2,1)	(2,2)	(1,3)	(3,1)
	Ref.20	4.454	6.992	7.045	8.890	9.782	9.960
	Ref.31	4.465	7.039	7.039	8.897	9.945	9.945
	Present (Ω_x)	4.463	7.028	7.043	8.893	9.938	9.953
	Present (Ω_y)	4.463	7.043	7.028	8.893	9.953	9.938
	Present (Ω)	4.463	7.035	7.035	8.893	9.945	9.945
	Difference (%)	0.044	0.056	0.056	0.044	0.000	0.000
1	Mode number	(1,1)	(1,2)	(2,1)	(2,2)	(3,1)	(1,3)
	Ref.20	4.529	7.008	7.136	8.936	9.787	10.036
	Ref.31	4.637	7.155	7.155	8.991	10.029	10.030
	Present (Ω_x)	4.648	7.098	7.223	8.993	10.093	9.968
	Present (Ω_y)	4.648	7.223	7.098	8.993	9.968	10.098
	Present (Ω)	4.648	7.160	7.160	8.993	10.030	10.033
	Difference (%)	0.237	0.069	0.069	0.022	0.009	0.029
10	Mode number	(1,1)	(1,2)	(2,1)	(2,2)	(1,3)	(3,1)
	Ref.31	5.346	7.768	7.768	9.537	10.552	10.563
	Present (Ω_x)	5.413	7.718	7.953	9.598	10.448	10.782
	Present (Ω_y)	5.413	7.953	7.718	9.598	10.782	10.453
	Present (Ω)	5.413	7.835	7.835	9.598	10.615	10.618
	Difference (%)	1.253	0.862	0.862	0.639	0.597	0.520
100	Mode number	(1,1)	(1,2)	(2,1)	(2,2)	(1,3)	(3,1)
	Ref.20	5.895	8.326	8.422	10.167	10.957	11.297
	Ref.31	5.901	8.442	8.442	10.253	11.307	11.333
	Present (Ω_x)	5.913	8.428	8.473	10.258	11.293	11.373
	Present (Ω_y)	5.913	8.473	8.478	10.258	11.373	11.293
	Present (Ω)	5.913	8.450	8.450	10.258	11.333	11.333
	Difference (%)	0.203	0.094	0.094	0.048	0.229	0.000
1000	Mode number	(1,1)	(1,2)	(2,1)	(2,2)	(1,3)	(3,1)
	Ref.31	6.011	8.585	8.585	10.424	11.495	11.522
	Present (Ω_x)	5.988	8.553	8.553	10.388	11.463	11.478
	Present (Ω_y)	5.988	8.553	8.553	10.388	11.478	11.463
	Present (Ω)	5.988	8.553	8.553	10.388	11.470	11.470
	Difference (%)	0.382	0.372	0.372	0.345	0.217	0.451

Table 5: Fundamental frequency parameter $2a\Omega = 2a\sqrt[4]{\rho h\omega^2/D_{11}}$ of rectangular orthotropic plates with three edges simply supported ($k^r_{\xi=-1} = k^r_{\xi=1} = k^r_{\eta=1} = 0$) and the edge at $\eta = -1$ rotationally restrained.

		$2a\Omega$				
b/a	$r_{\eta=-1}$	Ref.31	Present (Ω)	Present (Ω_x)	Present (Ω_y)	Difference (%)
0.5	0	7.530	7.523	7.523	7.523	0.092
	1	7.690	7.700	7.588	7.813	0.130
	10	8.250	8.308	8.198	8.418	0.703
	∞	8.705	8.695	8.695	8.695	0.114
1.0	0	4.917	4.918	4.918	4.918	0.020
	1	4.954	4.960	4.933	4.988	0.121
	10	5.114	5.128	5.088	5.168	0.273
	∞	5.289	5.278	5.278	5.278	0.207
1.5	0	4.126	4.128	4.128	4.128	0.048
	1	4.139	4.138	4.128	4.148	0.024
	10	4.202	4.208	4.188	4.228	0.142
	∞	4.292	4.288	4.288	4.288	0.093

5. Conclusion

In this study, the dynamic stiffness matrix (DSM) based on the extended separation-of-variable (SOV) type solution has been developed for the vibration analysis of an orthotropic rectangular plate with general homogeneous boundary conditions.

Instead of solving highly nonlinear eigenvalue equations involved in the SOV methods, the extended SOV type solution is adopted to construct the dynamic stiffness matrices. Several novel techniques have proposed to solve the eigenvalue problem and mode shape computation. The challenge of determining the fully clamped frequencies using the Wittrick-Williams (W-W) algorithm is resolved by finding the simply supported frequencies, whose closed-form expression can be easily derived based on the SOV method.

Classical boundary conditions, such as guided, simply supported, clamped, and free edges, can be realized by setting the translational springs (k_ξ^v) and rotational springs (k_ξ^r) along the plate edges to either zero or infinity. Numerical experiments have validated accuracy of this approach for these boundary conditions. The results shows that the SOV type solution can also be extended to handle elastically restrained boundary conditions. Despite certain approximations inherent in some elastically restrained cases, the maximum percentage error across all numerical experiments remains within 1.25%. This may occur because the SOV type solution used is derived from the weak-form governing equation, which is based on Rayleigh's principle.

Since the SOV type solution $\phi(\xi)\psi(\eta)$ consists of only a single term for each mode order, unlike the infinite series expansions used in the traditional DSM, each eigenvalue solution can be explicitly expressed. This suggests the potential for obtaining more concise solutions for assembled plate structures compared to traditional DSM methods.

Appendix A Integral parameters

The integral parameters I_1, I_2, I_3, and I_4 are defined as follows:

$$
\begin{aligned}
I_1 &= \int_0^1 \psi^2 \, d\eta \\
&= (B_1^2 + B_2^2 - B_3^2 + B_4^2) + \frac{-B_1^2 + B_2^2}{2\alpha_2} \sin(2\alpha_2) + \frac{B_3^2 + B_4^2}{2\beta_2} \sinh(2\beta_2) \\
&\quad + \frac{4(\alpha_2 B_2 B_4 + \beta_2 B_1 B_3)}{\alpha_2^2 + \beta_2^2} \sin(\alpha_2) \cosh(\beta_2) \\
&\quad + \frac{4(-\alpha_2 B_1 B_3 + \beta_2 B_2 B_4)}{\alpha_2^2 + \beta_2^2} \cos(\alpha_2) \sinh(\beta_2).
\end{aligned}
\tag{A.1}
$$

$$
\begin{aligned}
I_2 &= \int_0^1 \left(\psi \frac{d^2\psi}{d\eta^2} \right) d\eta \\
&= \left(-\alpha_2^2 B_1^2 - \alpha_2^2 B_2^2 - \beta_2^2 B_3^2 + \beta_2^2 B_4^2 \right) \\
&\quad + \frac{\alpha_2 (B_1^2 - B_2^2)}{2} \sin(2\alpha_2) + \frac{\beta_2 (B_3^2 + B_4^2)}{2} \sinh(2\beta_2) \\
&\quad + \frac{2(-\alpha_2^2 + \beta_2^2)(\alpha_2 B_2 B_4 + \beta_2 B_1 B_3)}{\alpha_2^2 + \beta_2^2} \sin(\alpha_2) \cosh(\beta_2) \\
&\quad + \frac{2(-\alpha_2^2 + \beta_2^2)(-\alpha_2 B_1 B_3 + \beta_2 B_2 B_4)}{\alpha_2^2 + \beta_2^2} \cos(\alpha_2) \sinh(\beta_2).
\end{aligned}
\tag{A.2}
$$

$$
\begin{aligned}
I_3 &= \int_0^1 \left(\frac{d\psi}{d\eta} \right)^2 d\eta \\
&= \alpha_2^2 B_1^2 + \alpha_2^2 B_2^2 + \beta_2^2 B_3^2 - \beta_2^2 B_4^2 \\
&\quad + \frac{\alpha_2 (B_1^2 - B_2^2)}{2} \sin(2\alpha_2) + \frac{\beta_2 (B_3^2 + B_4^2)}{2} \sinh(2\beta_2) \\
&\quad + \frac{4\alpha_2 \beta_2 (\alpha_2 B_1 B_3 - \beta_2 B_2 B_4)}{\alpha_2^2 + \beta_2^2} \sin(\alpha_2) \cosh(\beta_2) \\
&\quad + \frac{4\alpha_2 \beta_2 (\alpha_2 B_2 B_4 + \beta_2 B_1 B_3)}{\alpha_2^2 + \beta_2^2} \cos(\alpha_2) \sinh(\beta_2).
\end{aligned}
\tag{A.3}
$$

$$
\begin{aligned}
I_4 &= \int_0^1 \left(\frac{d^2\psi}{d\eta^2}\right)^2 d\eta \\
&= \left(\alpha_2^4 B_1^2 + \alpha_2^4 B_2^2 - \beta_2^4 B_3^2 + \beta_2^4 B_4^2\right) \\
&\quad + \frac{\alpha_2^3(-B_1^2 + B_2^2)}{2}\sin(2\alpha_2) + \frac{\beta_2^3(B_3^2 + B_4^2)}{2}\sinh(2\beta_2) \\
&\quad + \frac{4\alpha_2^2\beta_2^2(-\alpha_2 B_2 B_4 - \beta_2 B_1 B_3)}{\alpha_2^2 + \beta_2^2}\sin(\alpha_2)\cosh(\beta_2) \\
&\quad + \frac{4\alpha_2^2\beta_2^2(\alpha_2 B_1 B_3 - \beta_2 B_2 B_4)}{\alpha_2^2 + \beta_2^2}\cos(\alpha_2)\sinh(\beta_2)
\end{aligned}
\tag{A.4}
$$

The integral parameters J_1, J_2, J_3, and J_4 can be obtained by replacing B_1 to B_4 by A_1 to A_4, respectively, and α_2 and β_2 by α_1 and β_1, respectively.

References

[1] Banerjee, J., Papkov, S., Liu, X., Kennedy, D., 2015. Dynamic stiffness matrix of a rectangular plate for the general case. Journal of Sound and Vibration 342, 177–199. doi:10.1016/j.jsv.2014.12.031.

[2] Banerjee, J.R., 1997. Dynamic stiffness formulation for structural elements: a general approach. Computers & Structures 63, 101–103. doi:10.1016/S0045-7949(96)00326-4.

[3] Biancolini, M.E., Brutti, C., Reccia, L., 2005. Approximate solution for free vibrations of thin orthotropic rectangular plates. Journal of Sound and Vibration 288, 321–344. doi:10.1016/j.jsv.2005.01.005.

[4] Boscolo, M., Banerjee, J., 2011. Dynamic stiffness elements and their applications for plates using first order shear deformation theory. Computers & Structures 89, 395–410. doi:10.1016/j.compstruc.2010.11.005.

[5] Fazzolari, F., Boscolo, M., Banerjee, J., 2013. An exact dynamic stiffness element using a higher order shear deformation theory for free vibration analysis of composite plate assemblies. Composite Structures 96, 262–278. doi:10.1016/j.compstruct.2012.08.033.

[6] Ghorbel, O., Casimir, J.B., Hammami, L., Tawfiq, I., Haddar, M., 2015. Dynamic stiffness formulation for free orthotropic plates. Journal of Sound and Vibration 346, 361–375. doi:10.1016/j.jsv.2015.02.020.

[7] Gorman, D.J., 2005. Free in-plane vibration analysis of rectangular plates with elastic support normal to the boundaries. Journal of Sound and Vibration 285, 941–966. doi:10.1016/j.jsv.2004.09.017.

[8] Han, F., Dan, D., Cheng, W., Zang, J., 2018. An improved wittrick-williams algorithm for beam-type structures. Composite Structures 204, 560–566. doi:10.1016/j.compstruct.2018.07.108.

[9] Kantorovich, L.V., Krylov, V.I., 1958. Approximate Methods of Higher Analysis. Interscience Publishers, New York.

[10] Kerr, A.D., 1968. An extension of the kantorovich method. Quarterly of Applied Mathematics 26, 219–229. doi:10.1090/qam/99857.

[11] Khov, H., Li, W.L., Gibson, R.F., 2009. An accurate solution method for the static and dynamic deflections of orthotropic plates with general boundary conditions. Composite Structures 90, 474–481. doi:10.1016/j.compstruct.2009.04.020.

[12] Laura, P.A., Saffell Jr, B.F., 1967. Study of small-amplitude vibrations of clamped rectangular plates using polynomial approximations. The Journal of the Acoustical Society of America 41, 836–839. doi:10.1121/1.1910414.

[13] Leissa, A.W., 1973. The free vibration of rectangular plates. Journal of Sound and Vibration 31, 257–293. doi:10.1016/S0022-460X(73)80371-2.

[14] Levy, M., 1899. Sur l'équilibre élastique d'une plaque rectangulaire. Comptes Rendus Acad. Sci. Paris 129, 535–539.

[15] Li, R., Zhong, Y., Tian, B., Liu, Y., 2009a. On the finite integral transform method for exact bending solutions of fully clamped orthotropic rectangular thin plates. Applied Mathematics Letters 22, 1821–1827. doi:10.1016/j.aml.2009.07.003.

[16] Li, W.L., 2004. Vibration analysis of rectangular plates with general elastic boundary supports. Journal of Sound and Vibration 273, 619–635. doi:10.1016/S0022-460X(03)00562-5.

[17] Li, W.L., Zhang, X., Du, J., Liu, Z., 2009b. An exact series solution for the transverse vibration of rectangular plates with general elastic boundary supports. Journal of Sound and Vibration 321, 254–269. doi:10.1016/j.jsv.2008.09.035.

[18] Liu, X., Banerjee, J., 2015. An exact spectral-dynamic stiffness method for free flexural vibration analysis of orthotropic composite plate assemblies–part i: Theory. Composite Structures 132, 1274–1287. doi:10.1016/j.compstruct.2015.07.020.

[19] Liu, X., Banerjee, J., 2016. Free vibration analysis for plates with arbitrary boundary conditions using a novel spectral-dynamic stiffness method. Computers & Structures 164, 108–126. doi:10.1016/j.compstruc.2015.11.005.

[20] Mukhopadhyay, M., 1979. Free vibration of rectangular plates with edges having different degrees of rotational restraint. Journal of Sound and Vibration 67, 459–468.

[21] Navier, L., 1823. Extrait des recherches sur la flexion des plans elastiques. Bull. Sci. Soc. Philomat. , 95–102.

[22] Timoshenko, S., 1940. Theory of Plates and Shells. McGraw-Hill Book Company.

[23] Wittrick, W.H., Williams, F.W., 1971. A general algorithm for computing natural frequencies of elastic structures. The Quarterly Journal of Mechanics and Applied Mathematics 24, 263–284. doi:10.1093/qjmam/24.3.263.

[24] Xing, Y., Li, G., Yuan, Y., 2022. A review of the analytical solution methods for the eigenvalue problems of rectangular plates. International Journal of Mechanical Sciences 221, 107171. doi:10.1016/j.ijmecsci.2022.107171.

[25] Xing, Y., Liu, B., 2009a. New exact solutions for free vibrations of rectangular thin plates by symplectic dual method. Acta Mechanica Sinica 25, 265–270. doi:10.1007/s10409-008-0208-4.

[26] Xing, Y., Sun, Q., Liu, B., Wang, Z., 2018. The overall assessment of closed-form solution methods for free vibrations of rectangular thin

plates. International Journal of Mechanical Sciences 140, 455–470. doi:10.1016/j.ijmecsci.2018.03.013.

[27] Xing, Y., Wang, Z., 2020a. An extended separation-of-variable method for the free vibration of orthotropic rectangular thin plates. International Journal of Mechanical Sciences 182, 105739. doi:10.1016/j.ijmecsci.2020.105739.

[28] Xing, Y., Wang, Z., 2020b. An improved separation-of-variable method for the free vibration of orthotropic rectangular thin plates. Composite Structures 252, 112664. doi:10.1016/j.compstruct.2020.112664.

[29] Xing, Y.F., Liu, B., 2009b. New exact solutions for free vibrations of thin orthotropic rectangular plates. Composite Structures 89, 567–574. doi:10.1016/j.compstruct.2008.11.010.

[30] Yuan, S., Ye, K., Williams, F., 2004. Second order mode-finding method in dynamic stiffness matrix methods. Journal of Sound and Vibration 269, 689–708. doi:10.1016/S0022-460X(03)00126-3.

[31] Zhang, S., Xu, L., Li, R., 2019. New exact series solutions for transverse vibration of rotationally-restrained orthotropic plates. Applied Mathematical Modelling 65, 348–360. doi:10.1016/j.apm.2018.08.033.

[32] Zhong, W.X., 1995. A new systematic methodology for theory of elasticity. Dalian University of Technology Press, Dalian , 182–187.

[33] Zhong, Y., Zhao, X.F., Li, R., 2013. Free vibration analysis of rectangular cantilever plates by finite integral transform method. International Journal for Computational Methods in Engineering Science and Mechanics 14, 221–226. doi:10.1080/15502287.2012.711424.